https://doi.org/10.5194/egusphere-2024-501
Preprint. Discussion started: 23 February 2024

Biomass burning sources control ambient particulate matter but traffic and industrial sources control VOCs and secondary pollutant formation during extreme pollution events in Delhi

Arpit Awasthi[1], Baerbel Sinha[1], Haseeb Hakkim[1], Sachin Mishra[1], Varkrishna Mummidivarapu[1], Gurmanjot Singh[1], Sachin D. Ghude[2], Vijay Kumar Soni[3], Narendra Nigam[3], Vinayak Sinha[1], Madhavan N. Rajeevan[4]

[1]Department of Earth and Environmental Sciences, Indian Institute of Science Education and Research Mohali, Sector 81, S.A.S Nagar, Manauli PO, Punjab, 140306, India
[2]Indian Institute of Tropical Meteorology, Pashan, Pune 411 008, Ministry of Earth Sciences, India
[3]India Meteorological Department, New Delhi 110 003, Ministry of Earth Sciences, India
[4]Ministry of Earth Sciences, Government of India, New Delhi 110 003, India

Correspondence to: Baerbel Sinha (bsinha@iisermohali.ac.in)

Abstract. Volatile organic compounds (VOCs) and particulate matter (PM) are major constituents of smog. Delhi experiences severe smog during post-monsoon season, but a quantitative understanding of VOCs and PM sources is still lacking. Here, we source-apportioned VOCs and PM, using a high-quality recent (2022) dataset of 111 VOCs, $PM_{2.5}$, and PM_{10} using positive matrix factorization. Contrasts between clean-monsoon and polluted-post-monsoon air, VOC source fingerprints, molecular-tracers, enabled differentiating paddy-residue burning from other biomass-burning sources, which has hitherto been impossible. Fresh paddy-residue burning and residential heating & waste-burning contributed the highest to observed PM_{10} (25 % & 23 %), $PM_{2.5}$ (23 % & 24 %), followed by heavy-duty CNG-vehicles 15 % PM_{10} and 11 % $PM_{2.5}$. For ambient VOCs, ozone, and SOA formation potentials, top sources were petrol-4-wheelers (20 %, 25 %, 30 %), petrol-2-wheelers (14 %, 12 %, 20 %), mixed-industrial emissions (12 %, 14 %, 15 %), solid fuel-based cooking (10 %, 10 %, 8 %) and road construction (8 %, 6 %, 9 %). Emission inventories tended to overestimate residential-biofuel emission (>2) relative to the PMF output. The major source of PM pollution was regional biomass burning, whereas traffic and industries governed VOC and secondary pollutant formation. Our novel source-apportionment method quantitatively resolved even similar biomass and fossil-fuel sources, offering insights into both VOC and PM sources affecting extreme-pollution events. It represents a notable advancement over current source apportionment approaches, and would be of great relevance for future studies in other polluted cities/regions of the world with complex source mixtures.

1 Introduction

The Delhi National Capital Region (NCR) is located in the Indo-Gangetic plains and experiences some of the highest air pollution events worldwide, exposing its inhabitants to hazardous air quality. New Delhi had the world's highest population-

https://doi.org/10.5194/egusphere-2024-501
Preprint. Discussion started: 23 February 2024

weighted annual average $PM_{2.5}$ exposures of 217.6 μgm^{-3} and the sixth-highest $PM_{2.5}$-attributable death (85 deaths per lakh) (Pandey et. al., 2021). India is currently among the world's foremost developing countries and Delhi being its capital has witnessed rapid population growth and urbanization in the past decade, but a significant fraction of the population still lacks access to cleaner technologies for cooking and heating (Thakur M. 2023, Fadly et. al., 2023). Delhi with a population of 31.7 million people (UN World Population Prospects 2022), continues to add more than six hundred thousand vehicles per year (2022 VAHAN-Ministry of Road Transport and Highways (MoRTH), Government of India). The sources of air pollutants over the region have received much attention recently and a number of source apportionment methods have been applied. Several studies have relied on chemical mass balance models (CMB) that are unable to sniff out unknown fugitive sources since their application rests on prior knowledge of all relevant sources and their source profiles (Prakash et al., 2021; Srivastava et al., 2008). Clearly, in a dynamic developing world megacity like Delhi, where wide disparities exist in terms of access to clean energy and waste disposal practices, and many activities continue to be carried out by the informal sector, the CMB approach may misattribute emissions only to known sources, with no possibility of identifying other major sources that may be active. While much information has come to light through previous aerosol mass spectrometry-based source apportionment studies, a key limitation of the previous studies has been an inability to distinguish between different similar types of fossil fuel and biomass-burning sources (Kumar et al., 2022; Mishra et al., 2023). The other major limitation of existing studies has been the piece-meal approach where either VOCs (Jain et. al., 2022) or PM or a subset thereof have been investigated and even these analyses are based on datasets that were acquired in 2019 or earlier, i.e. pre-COVID19 period after which significant changes have been implemented. For example, the Bharat Stage VI which complies with the Euro VI norms was implemented in 2018 in Delhi and 2019 for Delhi NCR (Gajbhiye et. al., 2023). This significant decision was prompted by the severe air pollution challenges faced by Delhi, particularly worsening around 2019 (Gajbhiye et. al., 2023). Still air pollution continues to pose major health risks. Overall, a continued lack of strategic knowledge and inability to pinpoint the exact sources and their contribution, hampers efforts to propose evidence-based strategies for mitigation of major sources. In our previous studies from another site in the Indo-Gangetic Plain (Pallavi et al., 2019; Singh et al., 2023), we demonstrated that source apportionment carried out by PMF when combined with measured VOC chemical fingerprints of sources, can distinguish and quantify the contribution of even similar types of sources (e.g. within traffic source: to distinguish 4-wheelers from 2-wheelers and diesel vehicles; and within biomass burning sources to distinguish paddy stubble burning from residential biofuel combustion). We improve upon those studies that were carried out on datasets acquired using a unity mass resolution VOC proton transfer reaction mass spectrometer by recent new data acquired using the latest state-of-the-art enhanced volatile range high mass resolution and high sensitivity PTR-TOF-10 K technology over Delhi (Mishra et al., 2024).

The dataset used for source apportionment in this study using the positive matrix factorization modeling includes the high sensitivity (few ppt), high mass resolution (>10000) real-time acquisition of 111 speciated volatile organic compounds measured (15th August 2022–26th November 2022) using a Proton Transfer Reaction Time of Flight Mass Spectrometer 10 K (PTR-TOF10K-MS) instrument in Delhi, along with hourly averaged $PM_{2.5}$ and PM_{10} measurements. This dataset is novel in that it contains all major known gas phase molecular tracers for varied sources and VOC profiles of major agricultural and

https://doi.org/10.5194/egusphere-2024-501
Preprint. Discussion started: 23 February 2024

urban sources extant over Indo-Gangetic Plain. The dataset covered the relatively cleaner monsoon season which provides a baseline air pollution over the city and the post-monsoon season when post-harvest agricultural paddy residue burning in the Indo-Gangetic Plain perturbs the atmospheric chemical composition by providing an additional source of VOC and PM emissions. This comprehensive approach ensured that the positive matrix factorization model, which provides the advantage of determining air pollution sources without any prior knowledge of the source fingerprints, was able to quantify the source contribution of different sources to the ambient VOC, $PM_{2.5}$, and PM_{10} mass concentrations reliably as its solutions are sensitive to contrasts in ambient time series data. The statistical solution obtained using the model were verified against real-world measured source profiles from the region and thus presents a significant advancement over previous PMF source apportionment studies reported from the Delhi-NCR region. Furthermore, by combining this molecular tracer-based methodology and analyses with additional air mass back trajectory and statistical analyses, we also constrain the location of the major pollution sources and regions and compare the results of our source apportionment study with two widely used gridded emission inventories in chemical transport models, namely the Emission Database for Global Atmospheric Research (EDGARv6.1) (Crippa et al., 2022), and the Regional Emission inventory in Asia (REAS v3.2.1 (Kurokawa & Ohara, 2020).

2. Methodology

2.1 Measurement site and meteorological conditions:

The new PTR-TOF-MS 10 K enhanced volatility range mass spectrometer, as well as the primary VOC dataset and site, have already been described and analyzed in detail in the companion paper (Mishra et al., 2024). Hence only a brief description of these aspects and complementary aspects such as the air mass flow trajectories at the site during the study period from August 2022 to November 2022 are provided below.

Ambient air was sampled into the instruments from the roof-top of a tall building (28.5896°N-77.2210°E) at ~35 m above ground, located within the premises of the Indian Meteorological Department (IMD) in Lodhi Road, New Delhi situated in Central Delhi. The sampling site is a typical urban area surrounded by green spaces, government offices, and residential areas, but not in the direct vicinity of any major industries and representative of the airflow patterns observed in Delhi seasonally. Figure 1 shows the location of the site and also 120 h back trajectories of air masses arriving at the site that were grouped according to the dominant synoptic regional scale transport into a) south-westerly (orange and yellow), b) north-westerly (light and dark blue), and c) south-easterly flow (light and dark red). Square boxes indicate the fetch region from which air masses typically reach the receptor site within 24 h for a given flow situation. The panels on the right side show the d) photosynthetic active radiation, e) daily fire counts in the fetch region (21-32°N, 72-88°E), f) temperature and relative humidity, and g) the ventilation coefficient and the sum of the daily rainfall during the study period (15th August 2022– 26th November 2022).

Wind speed, wind direction, ambient temperature, relative humidity, and photosynthetic active radiation were measured using meteorological sensors (Campbell Scientific portable sensors equipped with CS215 RH and temperature sensor, PQS1 PAR sensor, TE525-L40 v rain gauge, Campbell Scientific Inc.). Boundary layer height was taken from the ERA5 dataset (Hersbach

https://doi.org/10.5194/egusphere-2024-501
Preprint. Discussion started: 23 February 2024

et al., 2023) and the ventilation coefficient was calculated as the product of the measured wind speed and boundary layer height. Fire counts were obtained using the Visible Infrared Imaging Radiometer Suite (VIIRS) 375 m thermal anomalies / active fire product data from the VIIRS sensor aboard the joint NASA/NOAA Suomi National Polar-orbiting Partnership (Suomi NPP) and NOAA-20 satellites, for high and normal confidence intervals only. The back trajectories in Fig. 1 showing the 5-day runs were obtained using Hysplit Desktop, version 5.2.1 (Stein et al., 2015; Rolph et al., 2017) with GFSv1 0.25° resolution meteorological fields as input data. The model was initialized every 3 hours (0, 3, 6, 9, 12, 15, 18 and 21 UTC) at 50 m above ground level for the year 2022 and trajectories were subjected to back trajectory cluster analysis via k-means clustering (Bow, 1984) with Euclidean distance metrics using the openair package (v2.11, Carslaw &. Ropkins, 2012). Three basic air transport situations occur at this site, namely from the South West (Fig. 1a), North-West (Fig. 1b), and South-East (Fig. 1c). These regional transport situations in the shared air-shed have been described for another receptor site located 300 km north of Delhi previously in great detail (Pawar et al, 2015). At Delhi, each of these large-scale flow patterns can occur with three different transport speeds; fast (darkest colour), medium (intermediate colour) and slow (lighter colour), resulting in 9 clusters.

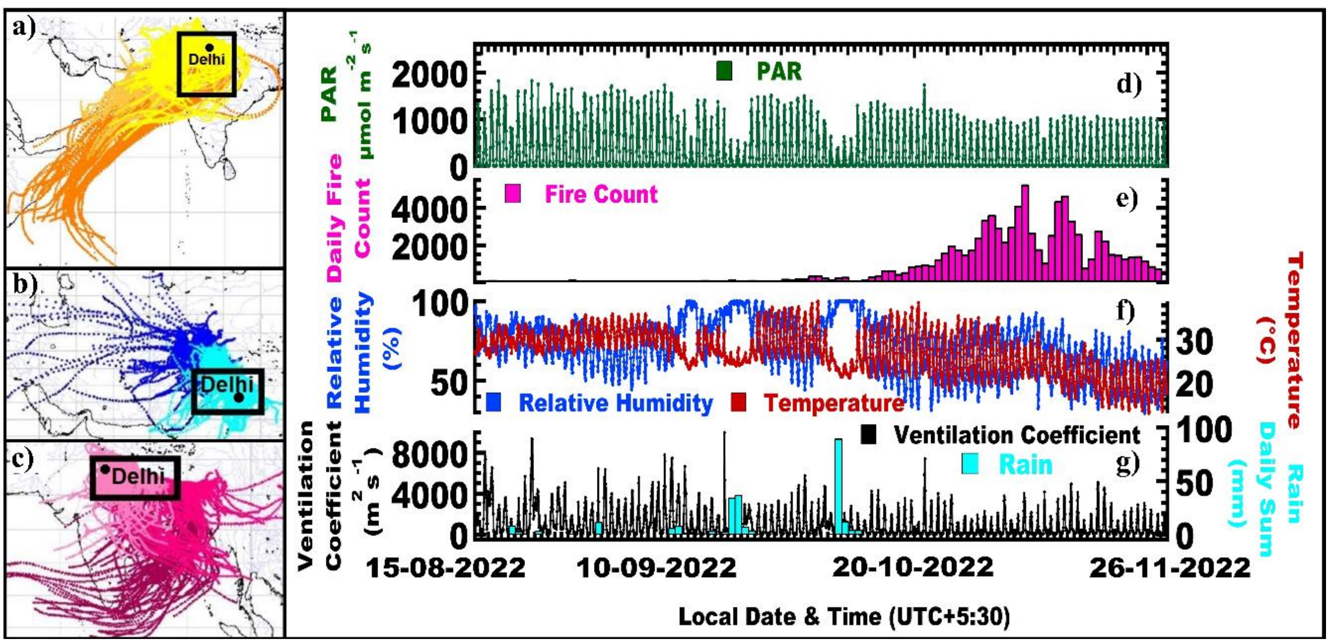

Figure 1: 120 h back trajectory air mass in blue reaching receptor site at Mausam Bhawan building (28.5896°N-77.2210°E, 50 m above ground level) grouped according to the dominant synoptic scale transport into a) South-Westerly, b) North westerly, and c) South-Easterly flow. Square boxes indicate the fetch region from which air masses typically reach the receptor site within 24 hrs for a given flow situation. On the right, panels show the d) solar radiation, e) daily fire counts in the fetch region, f) temperature and relative humidity, and g) the ventilation coefficient and the sum of the daily rainfall for the study period.

https://doi.org/10.5194/egusphere-2024-501
Preprint. Discussion started: 23 February 2024

During the monsoon season, the air masses from the south-west direction (western arm of the monsoon) were more prevalent than air masses reaching the site form the south-east (Bay of Bengal arm of the monsoon). During the post-monsoon season air masses remain confined over the NW-IGP for prolonged periods and primarily reach the site from the north-west (Fig. 1b), except during the passage of western disturbances (05.10-10.11.2022 and 04.11-10.11.2022), which result in brief periods with south westerly and southeasterly flow and rain (Fig. 1g). Figure 1e shows that paddy residue burning of short-duration varieties commences even before the monsoon withdrawal on 29th September 2022, however, the burning peaks during the harvest of late varieties in late October and early November. During this period a drop in temperature (Fig. 1f) and increased fire activity (Fig. 1e) results in the build-up of a persistent haze layer leading to suppressed solar radiation (Fig. 1d). This is associated with prolonged periods of poor ventilation (Fig. 1g).

2.2 Measurement of Volatile Organic Compounds, trace gases, and $PM_{2.5}$ and PM_{10} mass concentrations

Measurements of volatile organic compounds were performed using a high mass resolution and high sensitivity proton transfer reaction time of flight mass spectrometer (PTR-TOF10k; model PT10-004 manufactured by Ionicon Analytik GmbH, Austria). Details pertaining to the characterization, calibration, and QA/QC of the acquired dataset have been provided in Mishra et al., 2024. It is worth mentioning again that as a significant improvement over other previous PTR-TOF-MS deployments in Delhi, the inlet system of the instrument used in this work was designed for sampling and detection of low volatility compounds. Compared to previous PTR-TOF-MS instruments deployed in Delhi, this instrument also had unprecedented higher mass resolution (greater than 10000 m/Δm(FWHM) for m/z ≥ 79 Th even reaching as high as 15000 at m/z 330) coupled with high detection sensitivity (~ 1 ppt or better for 60 s averaged data), providing unprecedented ability for identification and quantification of new ambient compounds. Mass spectra were acquired over the m/z 15 to 450 amu range at a frequency of 1 Hz. Table S1 lists information pertaining to m/z, compound names and sources supported by references to previous studies where available, averaged ambient mass concentrations and classification of the species as weak or strong for the PMF model runs.

Thermofisher Scientific 48i (IR filter correlation-based spectroscopy), 43i (pulsed UV fluorescence), 49i (UV absorption photometry), and 42i trace level air quality analyzers (chemiluminescence) were used to quantify carbon monoxide (CO), ozone (O_3), and NO and NO_2, respectively. The overall uncertainty of the measurements was less than 6 %. Measurements of $PM_{2.5}$ and PM_{10} were made using Thermofisher Scientific Model 5014i series which is based on the beta-attenuation technique. Technical details pertaining to QA/QC of these instruments have been comprehensively described in our previous works (Chandra and Sinha, 2016; Kumar et al., 2016; Sinha et al., 2014). Carbon dioxide and methane were measured using a cavity ring down spectrometer (Model G2508, Picarro, Santa Clara, USA). The overall uncertainty of these measurements was below 4 % and technical details pertaining to the instrument are available in Chandra et al., 2018.

https://doi.org/10.5194/egusphere-2024-501
Preprint. Discussion started: 23 February 2024

2.3 Positive matrix factorization (PMF) model analysis

The US EPA PMF 5.0 (Paatero et al., 2002, 2014; Paatero & Hopke, 2009; Noris et al., 2014) was applied to a sample matrix of 2496 hourly observations and 111 VOC species, with S/N greater than 2.0 were all designated as strong species (94) and others as weak species (17). The total VOC mass was included as a weak species. $PM_{2.5}$ and PM_{10} were included as additional weak species in the model. This inclusion allows us to source apportion PM with the help of co-emitted gaseous chemical tracers. The specified uncertainty for weak species is tripled by the PMF model, to limit the influence of such species on the PMF solution.

The EPA PMF 5.0 is a multivariate factor analysis tool and a receptor model that divides the data matrix Xij (time series of measured concentrations of VOCs with i distinct observations and j measured species) into two matrices, Fkj (source fingerprint) and Gik (source contribution), along with a residual matrix, Eij, using the simultaneous application of the linear least square method in multiple dimensions.

$$\mathbf{X}_{\mathbf{ij}} = \sum_{k=1}^{p} \mathrm{G}_{\mathbf{ik}} \times \mathbf{F}_{\mathbf{kj}} + \mathbf{E}_{\mathbf{ij}} \qquad (1)$$

The user must provide the number of variables or sources (k). To determine the number of VOC sources the model can resolve in this atmospheric environment, the model was run with 3 to 12 factors. Figure 2 shows how the percentage of total VOC, $PM_{2.5}$, and PM_{10}, attributable to various sources changes when the number of factors increases from 3 to 12, while Fig. S1a-c illustrates the evolution in the factor contribution time series, source profile, and percentage of species explained by different sources when the number of factors in the PMF increases.

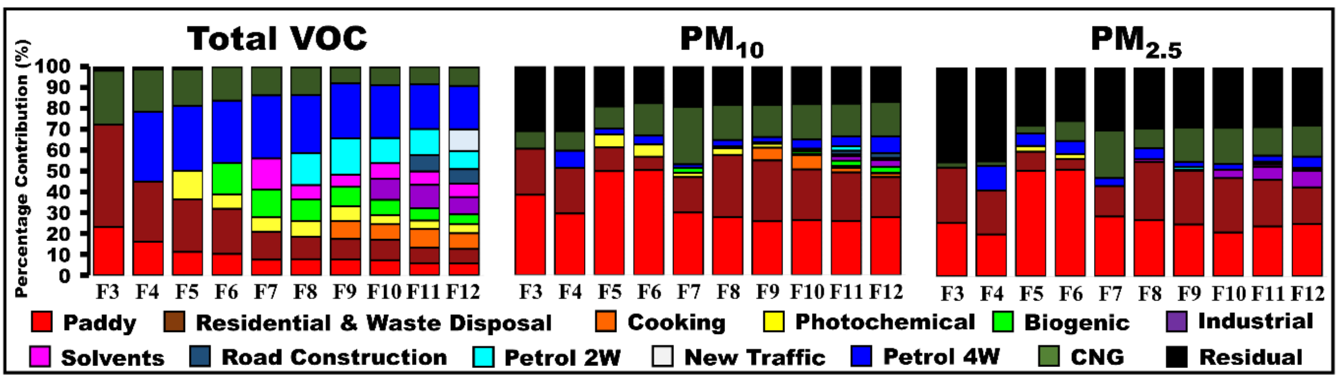

Figure 2: Percentage of the total VOC, PM_{10} and $PM_{2.5}$ mass explained by each factor in the PMF model output results when the number of PMF factors in the model is increased from 3 to 12. The balance to 100 % shown in black indicates the percentage share of the total mass in the PMF residuals.

While the three major traffic factors namely; CNG, petrol 4-wheeler, and petrol 2-wheeler are completely resolved with the 8 factors solution, three major biomass-burning related sources namely paddy residue burning, heating, and waste burning, and solid fuel-based cooking are separated with a 9-factors solution. Mixed industrial emissions are separated from solvent usage

https://doi.org/10.5194/egusphere-2024-501
Preprint. Discussion started: 23 February 2024

and other evaporative emissions with a 10-factor solution, Road construction activity emerges as a separate source with an 11-factor solution. While attempting to resolve 12-factors, the model splits transport sector emissions into four separate factors. However, this new transport sector factor shows a time series correlation (R=0.8) with the petrol 4-wheeler factor, and the 12-factor solution was found to be rotationally unstable during bootstrap runs, indicating that the model cannot resolve more than 11 factors with the available VOC tracers. The 12-factor solution also hardly improves the Qrobust/Qtheoretical and Qtrue/Qtheoretical ratio (Fig. S2). Therefore, the 11-factor solution was analyzed further. The model was run in the constrained model, elaborately described in Sarkar et. al., (2017) and Singh et al., (2023). The rotational ambiguity can be reduced using this option with the aid of prior knowledge. In our constrained run, we have pulled down primary emissions (acetonitrile, toluene, C8 aromatics, and C9 aromatics) in the biogenic and photochemical factors. We also pulled down the top-7 strongest nighttime plumes contaminating the biogenic and photochemical factors. In addition, we pulled up the highest plume event for all the anthropogenic emission-related factors as detailed in Table S2 The overall penalty to Q (the object function) was 4.9 %, which is within the recommended limit of 5 % (Norris et al., 2014; Rizzo & Scheff, 2007). The model uncertainty was assessed using bootstrap runs. The constrained model was found to be rotationally stable and robust with 100 % of all bootstrap runs for each individual factor mapped onto the base factor with R>0.6 and no unmapped bootstraps.

2.4 Calculation of the ozone formation potential, Secondary organic aerosol formation and volatility

T The contribution of VOCs to ozone production was derived using the maximum incremental reactivity (MIR) (Carter, 2010) using the following equation

$$OFP = \sum(c_i MIR_i) \qquad (2)$$

where ci is the measured concentration of VOC species i and MIRi is the maximum incremental reactivity of VOC species i. The Secondary Organic Aerosol Production (SOAP) was determined using the following equation

$$SOAP = \sum(c_i SOAP_i) \qquad (3)$$

SOAPi values were calculated with the SOA yields for high NOx emission environments reported in Table S3 according to the equation of Derwent et al., (1998, 2010), as Delhi being a megacity is a high NOx emission environment. When introduced to the ambient environment, each VOC species' ability to make SOA is evaluated in relation to the amount of SOA same mass of toluene would make which is represented by the SOAPi.

The saturation vapour pressure of VOCs was calculated using EPA EPI Suite v4.1 (MPBPWINv.1.43; KOAWIN v.1.00) provided by the US Environmental Protection Agency (US EPA, 2015) according to the method described in Li et al., (2016). The vapour pressure of liquids and gases is estimated using the average of the Antoine method (Lyman et al., 1990) and the modified Grain method (Lyman 1985). The vapour pressure is then converted to saturation mass concentration C_0 in μgm^{-3} using the following equation:

$$C_0 = \frac{M\, 10^6\, p_0}{760\, R\, T} \qquad (3)$$

https://doi.org/10.5194/egusphere-2024-501
Preprint. Discussion started: 23 February 2024

wherein M is the molar mass [g mol^{-1}], R is the ideal gas constant [8.205 x 10^{-5} atm K^{-1} mol^{-1} m^{3}], p_0 is the saturation vapor pressure [mm Hg], and T is the temperature (K). Organic compounds with $C_0 > 3 \times 10^6$ µgm^{-3} are classified as VOCs while compounds with $300 < C_0 < 3 \times 10^6$ µgm^{-3} as Intermediate VOCs (IVOCs).

2.5 Comparison of existing emission inventories with PMF derived output

The observational data was grouped according to the predominant airflow into a south-westerly, north-westerly, and south-easterly group, and the fetch region from which air masses would reach the receptor site was determined for each group separately spanning latitude 21–31 ̊N and longitude 72–82 ̊E, latitude 28–32 ̊N and longitude 72–80 ̊E and latitude 25–30 ̊N and longitude 75–88 ̊E, respectively, for the three flow regimes. Two gridded emission inventories namely the Emission Database for Global Atmospheric Research (EDGARv6.1) for the year 2018 (Crippa et al., 2022), and the Regional Emission inventory in Asia (REAS v3.2.1) for the year 2015 (Kurokawa & Ohara, 2020) were filtered for these three fetch regions to compare PMF results with the emission inventory. For the purpose of emission inventory comparison of anthropogenic sources, biogenic emissions and the photochemistry factor were removed from the PMF output, while the solid fuel-based cooking and residential heating and waste burning emissions were summed up in residential & waste management while CNG and Petrol 2 & 4-wheeler factors are combined into the consolidated transport sector emissions.

3 Results and Discussions:

3.1 Validation of the PMF output and contribution of individual sources to the total VOC, $PM_{2.5}$ and PM_{10} mass and secondary pollutant formation.

The source identity of the PMF factors was confirmed by matching the normalized PMF factor profiles with normalized source fingerprints of grab samples collected from the potential sources. To facilitate the comparison of emission factors with the unit g/kg with the PMF output with the unit µgm^{-3} both were also normalized by dividing each species' mass/emission factor by the mass/emission factor of the most abundant species in a given fingerprint. The PMF factor profile matched best against source samples collected from burning paddy fields (Kumar et al., 2020) for the paddy residue burning factor. The cooking factor matched emissions from a cow-dung-fired traditional stove called angithi (Fleming et al., 2018). The residential heating & waste burning factor had a source fingerprint matching emission from leaf litter burning (Chaudhary et. al., 2022), waste burning (Chaudhary et. al., 2021), and cooking on a chulha fired with a mixture of firewood and cow dung (Fleming et al., 2018). The factors identified as CNG, petrol 4-wheelers, and petrol 2-wheelers matched tailpipe emissions of the respective vehicle types and fuels (Hakkim et al., 2021). The road construction factor matched the source fingerprint of asphalt mixture plants, asphalt paving (Li et. al., 2020), and road construction vehicles (Che et. al., 2023).
The factors identified as solvent usage and evaporative emissions matched ambient air grab samples from Munirka furniture market and Dhobighat at Akshar Dham. The factor identified as industrial emissions showed the greatest similarity to ambient

https://doi.org/10.5194/egusphere-2024-501
Preprint. Discussion started: 23 February 2024

air grab samples from the vicinity of the Okhla waste to the energy plant and industrial area at Faridabad. The biogenic factor showed the greatest similarity to plant chamber source profiles of Mangifera indica (Datta et al., 2021), leaf wounding compounds released from Populus tremula (Portillo-Estrada et al., 2015) as well as ambient BVOC measurements in an orange orchard (Park et al., 2013).

https://doi.org/10.5194/egusphere-2024-501
Preprint. Discussion started: 23 February 2024

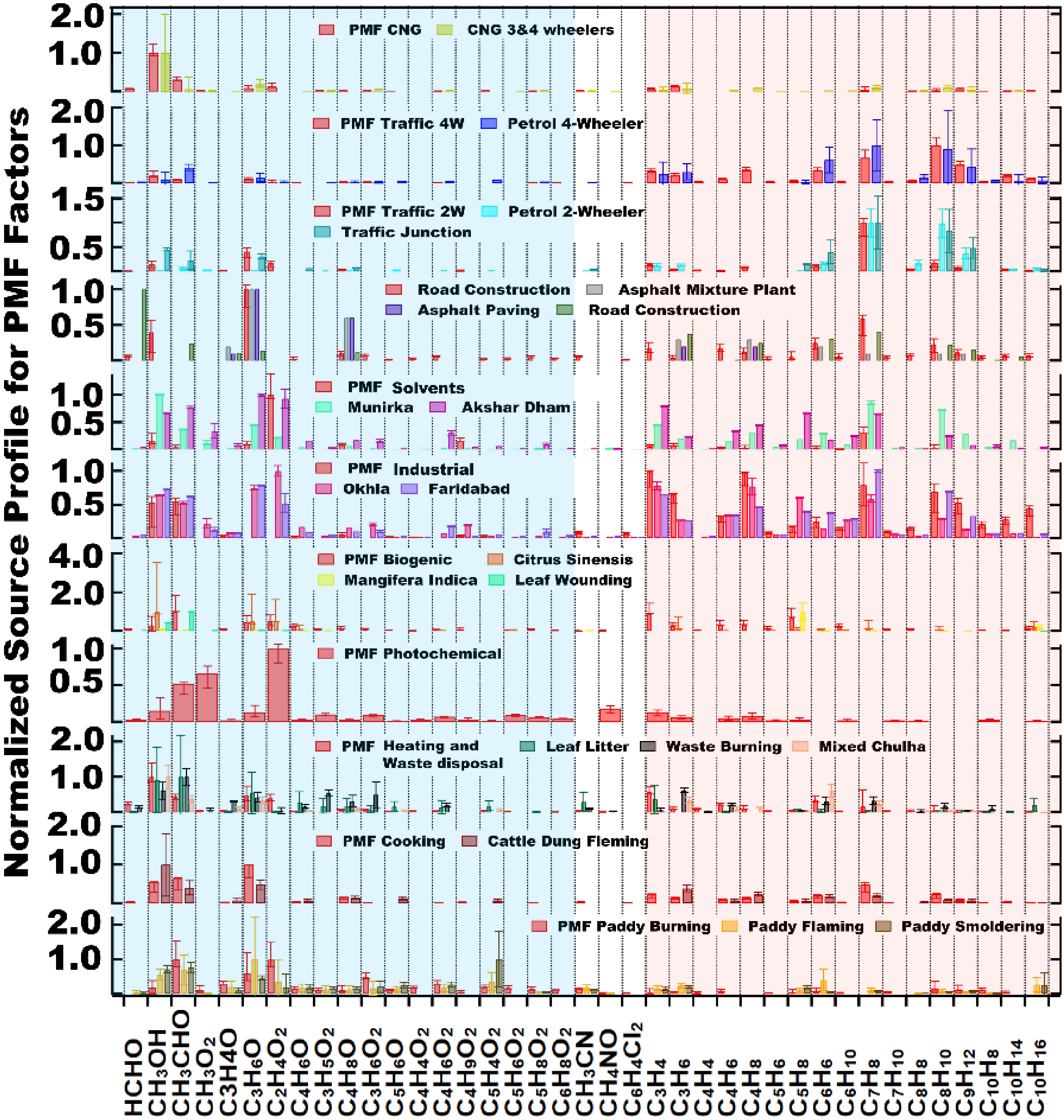

Figure 3: PMF factor profile of the 11 factors identified. The normalized source fingerprints of the PMF factors (red) and source fingerprint of grab samples collected at the source (in various colours). The Error bars indicate the 2σ uncertainty range from the bootstrap runs for PMF factor profiles and the 1σ fire-to-fire or vehicle-to-vehicle variability of the emission factors for source samples.

https://doi.org/10.5194/egusphere-2024-501
Preprint. Discussion started: 23 February 2024

Figure 3 shows the source profile of the eleven factors that our PMF analysis resolved, which in descending ranking of their contribution to the total VOC mass concentration and ozone formation potential (Fig. 4 a & d), were petrol 4-wheeler vehicles (20 % & 25 %), petrol 2-wheeler vehicles (14 % & 12 %), industries (12 % & 14 %), cooking (10 % & 10 %), CNG vehicles (9 % & 7 %), road construction (8 % & 6 %), heating & waste disposal (7 % & 6 %), solvents usage (6 % & 3 %), biogenic emissions (4 % & 6 %), paddy residue burning (6 % & 6 %), and photochemistry (4 % & 3 %) respectively. In the megacity of Delhi, all transport sector sources combined contributed 43 % to the total VOC burden while they contributed only 24 % at a suburban site in the NW-IGP (Singh et al., 2023). On the other hand, the contribution of both, paddy residue burning (6 %) and total residential sector solid fuel usage and waste disposal (17 % in Delhi and 18 % in Mohali) to the VOC burden during post-monsoon season was similar at both sites.

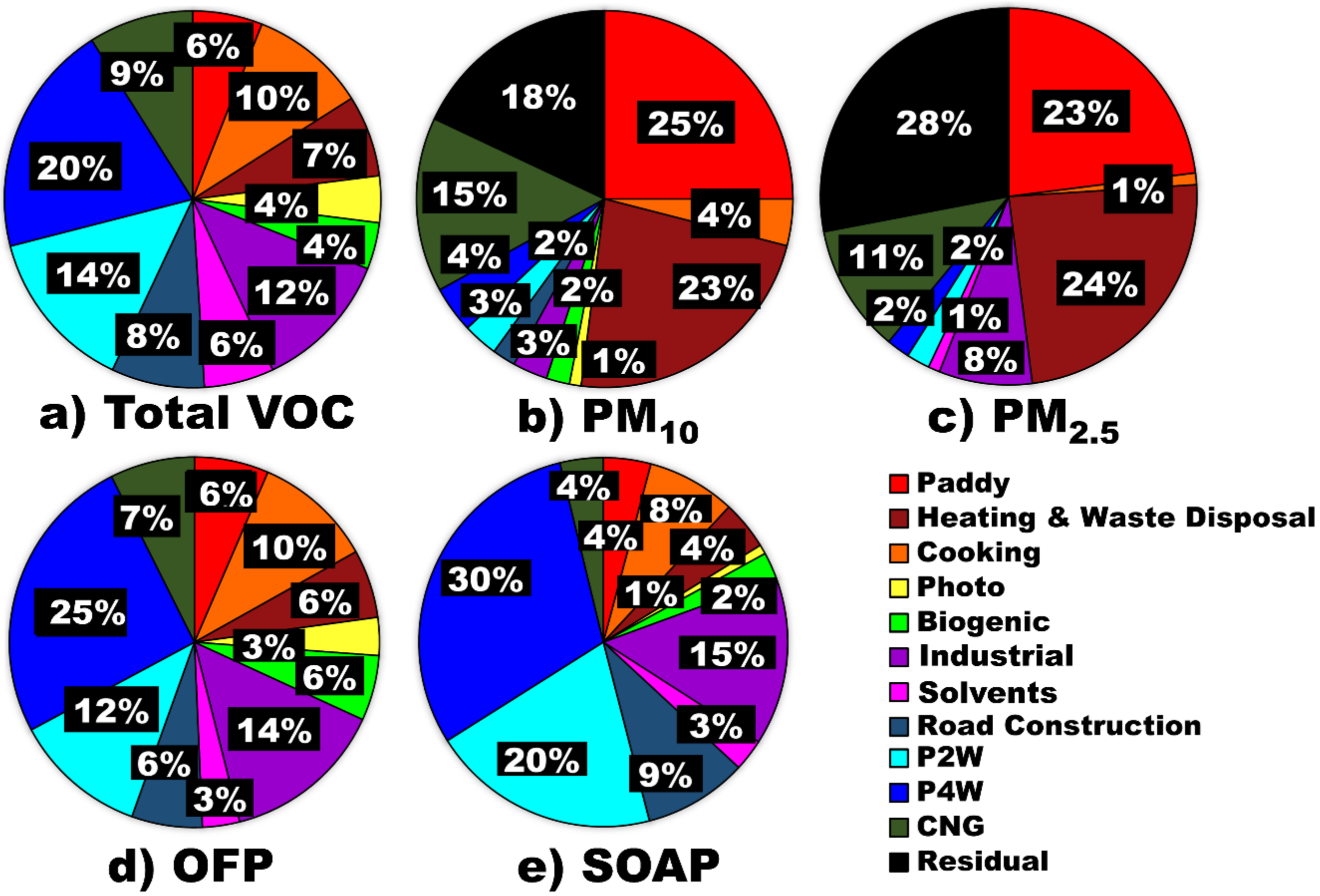

Figure 4: Source contribution of the 11 sources to the (a) total ambient VOC mass loading, (b) PM_{10} mass loading and (c) $PM_{2.5}$ mass loading (d) ozone formation potential and (e) SOA formation potential.

https://doi.org/10.5194/egusphere-2024-501
Preprint. Discussion started: 23 February 2024

The contribution of the different factors to the SOA formation potential (Fig. 4 e) stands in stark contrast to their contribution to primary particulate matter emissions. Secondary organic aerosol formation potential was dominated by the transport sector which contributed 54 % to the SOA formation potential (petrol 4-wheeler vehicles 30 %, petrol 2-wheeler vehicles 20 %, CNG vehicles 4 %). Minor contributors to SOA formation were industries (15 %), road construction (9 %), and solid fuel-based cooking (8 %). All other sources contributed <5 % of each of the SOA formation potential. Direct PM_{10} and $PM_{2.5}$ emissions were dominated by biomass burning (Fig. 4 b & c). Paddy residue burning was one of the largest contributors to the total observed PM_{10} (25 %) and $PM_{2.5}$ (23 %) mass concentrations in Delhi. An earlier WRF-Chem-based study with the FINNv1.5 inventory had attributed 20 % of the $PM_{2.5}$ burden to this source for the year 2018 (Kulkarni et al., 2020). Residential heating & waste burning contributed 23 % & 24 % to the PM_{10} and $PM_{2.5}$ burden, respectively. CNG-fuelled vehicles also contribute significantly to the PM_{10} (15 %) and $PM_{2.5}$ (11 %) burden. A significant share of the PM_{10} (18 %) and $PM_{2.5}$ (28 %) burden is associated with the residual and not directly linked to combustion tracers. This share can likely be attributed to windblown dust arriving at the site through long-range transport (Pawar et al., 2015) and to secondary organic, and secondary inorganic aerosols such as ammonium sulfate and ammonium nitrate. Due to the complex relationship of secondary aerosol with gas-phase precursors and emission tracers, VOC tracers are not a suitable tool to source-apportion this aerosol component. Meteorological conditions, homogeneous, heterogeneous, and multiphase chemistry control how fast primary emissions are converted to secondary aerosol. To explain the source of those species, one also needs to invoke the physicochemical and thermodynamical properties of the aerosol. (Acharja et al., 2022).

3.2 Detailed discussion of individual emission sources

3.2.1 Factor 1: Paddy residue burning

The VOC profile of this factor (Fig. 3) matches source samples collected from burning paddy fields (Kumar et al., 2021). In descending rank of mass contribution, acetaldehyde m/z45.030 (1.6 μgm^{-3}), acetic acid m/z61.025 (1.6 μgm^{-3}), acetone + propanal m/z59.046 (1.0 μgm^{-3}), hydroxyacetone m/z75.042 (0.8 μgm^{-3}), acrolein m/z57.030 (0.5 μgm^{-3}), diketone m/z 87.043 (0.5 μgm^{-3}) and furfural m/z97.027 (0.3 μgm^{-3}) contributed most to the total VOC mass of this factor. Figure 5 shows that the 24-h averaged factor contribution time series has the highest cross correlation with same day fire counts (R=0.8), while hourly average source contributions correlate most with $PM_{2.5}$ (0.7), PM_{10} (0.7) and CO (R=0.5) (Table S4). The high correlation with same day fire counts points towards nearby fire activity as the dominant source of paddy burning related pollution in the Delhi NCR. A recent study from Punjab indicated, that the largest PM enhancements at a receptor are caused by fire occurring within 50 km radius around the receptor site (Pawar & Sinha 2022). Figure S4 shows that the $PM_{2.5}$ and PM_{10} mass loadings at the receptor site increased by 0.027 and 0.047 μgm^{-3}, respectively for each additional fire count within the 24-hour fetch region whenever the trajectories are arriving through north-west and south-west region. It is very interesting to note that the incremental increase in $PM_{2.5}$ and PM_{10} mass loadings for each additional fire count were almost four times higher than the former regions when the trajectory fetch region was south-east with 0.109 and 0.192 μgm^{-3} respectively.

https://doi.org/10.5194/egusphere-2024-501
Preprint. Discussion started: 23 February 2024

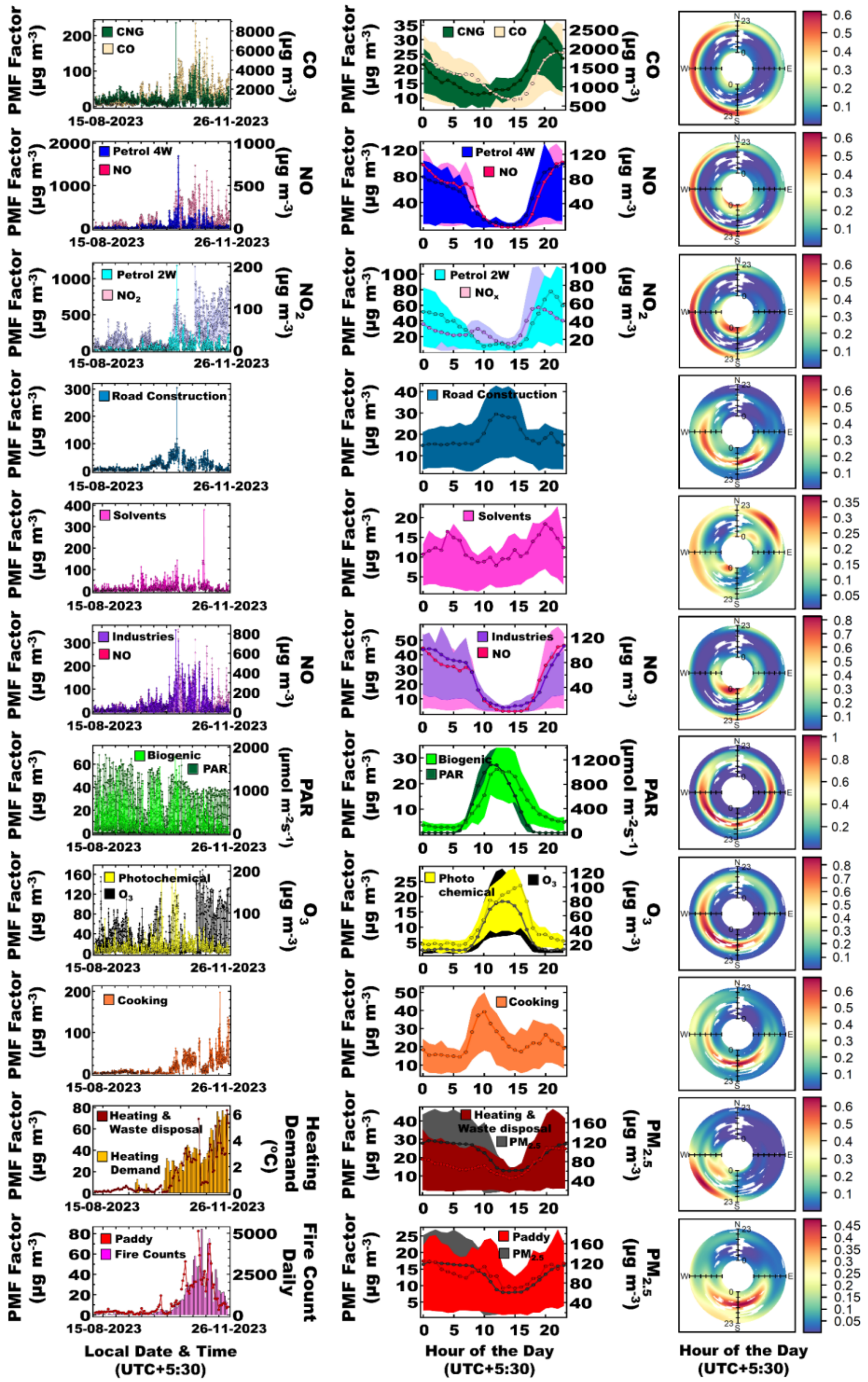

295 **Figure 5: Time series of each factor in µg m−3 (left column) with respective normalized diurnal profiles (centre column) and polar plots (right column) depicting the conditional probability of a factor having a mass contribution above the 75th percentile during a certain hour of the day between midnight (centre of rose) and 23:00 local time (outside of rose) from a certain wind direction.**

Figure 6 demonstrates that paddy residue burning (labeled agriculture to compare with EIs) is an equally important source of particulate matter in air masses reaching the receptor from the North-Western IGP (24 % and 27 % of $PM_{2.5}$ and PM_{10}, respectively) and the South-Eastern IGP (24 % and 27 % of $PM_{2.5}$ and PM_{10}, respectively), despite the much lower fire counts over the South-Eastern IGP (17,810), when compared to the North Western IGP (61,334). This indicates that either fires to the SE are burning closer to the receptor site or the fire detection efficiency in this fetch region is lower due to factors such as the prevailing burning practices (Liu et al., 2019) and landholding sizes. Regional gradients in fire detection efficiency can complicate attempts to model air quality with the help of fire-count-based emission inventories (Kulkarni et al., 2020). Paddy residue burning contributed less to the PM burden in air masses reaching from Central and South-West India (19 % and 17 % of $PM_{2.5}$ and PM_{10}, respectively). Its importance as a PM source stands in stark contrast to its minor contribution to the overall VOC mass loading in Delhi (6 %). In Mohali, Punjab, this source was also found to only contribute 6 % to the VOC burden in October and November (Singh et al., 2023).

Figure S3(a) shows that this factor explained the largest percentage share of O-heteroarene compounds such as furfural m/z97.027 (46 %), methyl furfural m/z111.042 (52 %), hydroxy methyl furfural m/z127.039 (44 %), furanone m/z85.027 (48 %), hydroxymethyl furanone m/z115.039 (38 %), furfuryl alcohol m/z 99.043 (39 %), furan m/z69.031 (38 %), methyl furans m/z83.047 (35 %), C2-substituted furans m/z97.063 (29 %), and C3-substituted furans m/z111.080 (27 %), which are produced by the pyrolysis of cellulose and hemicellulose, and have previously been detected in biomass burning samples (Coggon et al., 2019; Hatch et al., 2015; 2017; Koss et al., 2018; Stockwell et al., 2015). Figure S3(a) also shows that this factor explains the largest share of the most abundant oxidation products that result from the nitrate radical-initiated oxidation of toluene as well as from OH-imitated oxidation of aromatic compounds under high NOx conditions, namely nitrotoluene m/z138.056 (30 %) and nitrocresols m/z154.052 (45 %) (Ramasamy et al., 2019), which indicates a certain degree of aging of the plumes. These nitroaromatic compounds are significant contributors to SOA and BrC, (Palm et al., 2020, Harrison et al., 2005). It also explains several other nitrogen containing VOCs such as nitroethane m/z76.045 (38 %), the biomass burning tracer acetonitrile m/z42/030 (21 %) and pentanenitrile m/z84.080 (44 %). The presence of pentanenitrile isomers in biomass burning smoke has previously been confirmed using gas chromatography-based studies (Hatch et al., 2015, Hatch et al., 2017). In addition the factor explains the largest percentage share of acrolein m/z57.030 (49 %), hydroxyacetone (41 %), cyclopentadienone m/z81.031 (31 %), cyclopentanone m/z85.063 (26 %), diketone m/z87.043 (35 %), pentanedione m/z101.059 (26 %), hydroxybenzaldehyde m/z123.043 (34 %), guaiacol m/z125.06 (32 %), and the levoglucosan fragment m/z145.0505 (43 %), many of these compounds are known to form during lignin pyrolysis (Hatch et al., 2015, Koss et al., 2018; Nowakowska et al., 2018), while dimethylbutenedial m/z113.059 (33 %), trimethylbutenedial m/z127.075 (26 %) are ring opening oxidation products of aromatic compounds (Zaytsev et al., 2019).

https://doi.org/10.5194/egusphere-2024-501
Preprint. Discussion started: 23 February 2024

3.2.2 Factor 2: Residential heating and waste disposal

The residential heating and waste disposal is the second largest particulate matter source at the receptor site and contributes 23 % and 24 % to the total PM_{10} and $PM_{2.5}$ mass loadings, respectively (Fig. 4). Emissions peak at nighttime (Fig. 5) and the factor contribution time series displays the largest cross-correlation with the 24 h averaged heating demand (R=0.8) (Fig. S5), PM_{10} (R=0.7), $PM_{2.5}$ (R=0.6), NO_2 (R=0.7) and CO (R=0.5) (Table S4). The lower correlation with NO (R=0.4) (Table S4), indicated that emissions are combustion-related but not always fresh. The source fingerprints (Fig. 3) show the greatest similarity of this with leaf litter burning, waste burning (Chaudhary et. al., 2021), and cooking on a chulha fired with a mixture of firewood and cow dung (Fleming et al., 2018) and the factor contribution time series is anti-correlated with temperature (R=-0.6) indicating that this combustion activity is primarily triggered by the need to keep warm. Figure S5 shows that the $PM_{2.5}$ and PM_{10} mass loadings at the receptor site increase by 13.9 µgm^{-3} and 22.3 µgm^{-3}, respectively for each degree increase in the 24-h average heating demand. Earlier studies have documented the strong seasonality of open waste burning emissions over Delhi as well as the diversity of fuel used in wintertime heating-related fires (Nagpure et al., 2015). This factor explains 7 % of the total VOC mass loading. The top contributors to the VOC mass of this factor are in descending rank of contribution: methanol m/z33.030 (2.4 µgm^{-3}), propyne m/z41.035 (1.4 µgm^{-3}) acetone + propanal m/z59.046 (1.1 µgm^{-3}), acetaldehyde m/z45.03 (1.1 µgm^{-3}), acetic acid m/z61.025 (1.0 µgm^{-3}) and benzene m/z79.052 (0.8 µgm^{-3}). Figure S3(a) shows thas this factor explains the largest percentage share of the total mass for formaldehyde (46 %) m/z31.014 and vinylacetylene + 1-buten-3-yne m/z53.035 (36 %), and the second largest percentage share of furfural (23 %), methyl furfural (15 %), furan (19 %), methyl furan (15 %), furanone (16 %) and acrolein (14 %). All these compounds are characteristic of biomass burning smoke (Hatch et al., 2015, Stockwell et al., 2015, Koss et al., 2018).

3.2.3 Factor 3: Solid fuel-based cooking

The cooking factor is a daytime factor and explains 10 % of the total VOC mass loading (Fig. 4) but only a negligible share of the total PM_{10} (≤4 %) burden. The source profile (Fig. 3) matched emissions from a cow-dung-fired traditional stove called angithi (Fleming et al., 2018). The activity peaks from 8 am to noon time, with a secondary peak in the early evening hours and persists throughout monsoon and post-monsoon season. In descending rank of mass contribution acetone + propanal (4.5 µgm^{-3}), acetaldehyde (2.9 µgm^{-3}), methanol (2.4 µgm^{-3}), toluene m/z93.069 (2.1 µgm^{-3}), the sum of C8 aromatics m/z107.085 (1.1 µgm^{-3}), propyne (1.1 µgm^{-3}) and benzene (0.9 µgm^{-3}) contribute most to this factor. Figure S3(a) shows that factor explains the largest percentage share of butanone m/z73.062 (28 %), pentanone m/z87.079 (28 %), acetaldehyde (28 %), acetone (26 %), and benzaldehyde m/z107.0486 (29 %). All these compounds are characteristic of biomass burning smoke (Hatch et al., 2015, Stockwell et al., 2015, Koss et al., 2018).

3.2.4 Factor 4: CNG

CNG-fuelled vehicles are identified as the third largest identified source of PM_{10} (15 %) and $PM_{2.5}$ (11 %) and contribute 9 % to the total VOC burden (Fig. 4). The high contribution of this source to the particulate matter burden confirms earlier emission-inventory-based estimates which flagged that non-tailpipe emissions such as brake and tire wear and road dust resuspension have become the dominant transport sector related particulate matter sources in the Delhi-NCR region (Nagpure et al., 2016). The study attributed a large share of these non-tailpipe emissions to buses and commercial vehicles that are typically fuelled by CNG. This is consistent with our results. In descending order methanol (8.1 μgm^{-3}), acetone + propanal (1.7 μgm^{-3}), toluene (0.9 μgm^{-3}), C-8 aromatic compounds (0.9 μgm^{-3}), butene m/z57.067 (0.8 μgm^{-3}), propene m/z43.051 (0.7 μgm^{-3}), and acetaldehyde (0.5 μgm^{-3}) contribute most to the VOC mass in this source. Figure S3(b) shows that the factor explains the largest percentage share of methanol m/z33.030 (41 %) and second largest percentage share of ethanol m/z47.0456 (22 %).

3.2.5 Factor 5: Petrol 4-wheeler factor

The source fingerprint of this source matched tailpipe emissions of petrol-fueled 4-wheelers (Hakkim et al., 2021) and is characterized, in descending rank of contribution, by C8-aromatics (7.6 μgm^{-3}), toluene (5.1 μgm^{-3}), C9-aromatics (3.7 μgm^{-3}), benzene (2.6 μgm^{-3}), butene + methyl tert-butyl ether (MTBE) fragment (2.6 μgm^{-3}), propyne (2.3 μgm^{-3}), propene (1.6 μgm^{-3}), methanol (1.6 μgm^{-3}) and C2-substituted xylenes + C4-substituted benzenes m/z135.118 (1.4 μgm^{-3}). Figure 5 shows that emissions peak in the evening between 7 pm and midnight with average VOC mass loadings >70 μgm^{-3} and reach the receptor site from most wind directions. Emissions are strongly correlated with NO (R=0.8), CO (R=0.7) and CO_2 (R=0.7) indicating the receptor site is impacted by fresh combustion emissions from this source. Figure S3(b) shows that the factor explains the largest percentage share of most aromatic compounds, namely C8-aromatics (54 %), toluene (52 %), C9-aromatics (52 %), C4-substituted benzene + C2-substituted xylene m/z135.118 (51 %), benzene (35 %), styrene m/z105.069 (27 %), methylstyrenes + indane m/z119.085 (29 %), and C2-substituted styrenes m/z133.102 (38 %) and a few oxygenated aromatic hydrocarbons such as methyl phenol isomers m/z109.064 (24 %) and methyl chavicol m/z149.096 (23 %). The fact that the factor explains the largest percentage share of ethanol m/z47.046 (29 %) and the Methyl tert-butyl ether (MTBE) fragment (30 %) can likely be attributed to ethanol blending and the use of MTBE in petrol (Achten et.al., 2001). This factor also explains the largest percentage share of several other hydrocarbons such as propyne (21 %), propene (26 %), cyclopentadiene m/z67.051 (24 %), hexene m/z85.099 (31 %), C_7H_6 m/z91.053 (29 %), C_7H_{10} m/z95.084 (26 %), cycloheptene m/z97.100 (26 %).

3.2.6 Factor 6: Petrol 2-wheeler factor

The source fingerprint of this source matched tailpipe emissions of petrol-based 2-wheelers (Hakkim et al., 2021) and is characterized, in descending rank of contribution, by toluene (9.4 μgm^{-3}), acetone + propanal (3.9 μgm^{-3}), C-8 aromatic compounds (1.7 μgm^{-3}), acetic acid (1.7 μgm^{-3}), propyne (1.5 μgm^{-3}), methanol (1.4 μgm^{-3}), benzene (1.3 μgm^{-3}), methyl tert-butyl ether (MTBE) fragment (0.9 μgm^{-3}) and C-9 aromatics m/z121.101 (0.7 μgm^{-3}). Figure 5 shows that emissions peak in

https://doi.org/10.5194/egusphere-2024-501
Preprint. Discussion started: 23 February 2024

the evening between 8 pm and 10 pm with average VOC mass loadings >50 µgm^{-3} and reach the receptor site from most wind directions. Emissions are strongly correlated with NOx (R=0.6), CO (R=0.6) and CO_2 (R=0.7), but have a lower correlation with NO (R=0.5) (Table S4) and a larger contribution of oxygenated compounds to the source profile indicating that the emissions have been photochemically aged. Figure S3(b) shows that this factor explains the largest percentage share of toluene (41 %), and a number of oxygenated aromatic compounds such as benzaldehyde m/z107.049 (30 %), tolualdehyde m/z121.064 (25 %), and phenol m/z95.045 (20 %). It also explains the largest percentage share of nitrobenzene m/z124.039 (31 %), cyclohexanone m/z99.079 (36 %), and vinyl chloride m/z62.997 (26 %). It also explains the second largest percentage share of benzene (17 %), vinylacetylene m/z53.035 (35 %), C_7H_6 (24 %), acetone + propanal (22 %), methoxy amine m/z48.048 (20 %) and butanoic acid/ethyl acetate m/z89.058 (16 %).

3.2.7 Factor 7: Mixed Industrial

This factor on average contributes >30 µgm^{-3} to the VOC burden throughout the night from 9 pm to 7 am (Fig. 5) and due to industrial point sources located in the wind sector S to SW of the receptor site. Emissions are most strongly correlated with CO (R=0.7), NO(R=0.7), CH4 (R=0.8), and CO_2 (R=0.8) indicating that the emissions are fresh and originate from combustion processes. This factor explains 12 %, 3 % and 8 % of the total VOC, PM_{10} and $PM_{2.5}$ mass loading at the receptor site, respectively. The main contributors towards the VOC mass in the mixed industrial factor, are in descending order of contribution propyne (2.3 µgm^{-3}), methyl tert-butyl ether (MTBE) fragment / butene (2.2 µgm^{-3}), toluene (1.8 µgm^{-3}), C-8 aromatic compounds (1.6 µgm^{-3}), propene (1.5 µgm^{-3}), acetaldehyde (1.2 µgm^{-3}),, methanol (1.2 µgm^{-3}), C-9 aromatics m/z121.1013 (1.2 µgm^{-3}) and the sum of monoterpenes (MT) m/z137.133 (1.0 µgm^{-3}). The source fingerprint is most similar to ambient air grab samples collected near the Okhla waste to energy plant and industrial area in Faridabad.

Figure S3(c) shows that the factor explains the largest percentage share of methanethiol m/z49.007 (72 %), a chemical used in the manufacture of the essential amino acid methionine, in the plastic industry and the manufacturing of pesticides, dichlorobenzene m/z146.977 (48 %), a chemical used in the synthesis of dyes, pesticides, and other industrial products and methoxyamine m/z48.048 (27 %). Analyses of the primary dataset by Mishra et al. (2024) also qualitatively inferred an industrial source for methanethiol and dichlorobenzenes. It also explains the largest percentage share of the sum of monoterpenes (MT) (44 %), camphor/pinene oxide m/z153.128 (43 %), santene m/z123.116 (26.0 %) the terpene fragment C_8H_{12} m/z109.100 (26 %), C_8H_{14} m/z111.116 (30 %), C_9H_{16} m/z 125.133 (24 %), cyclohexene m/z83.084 (24 %) and cyclopentylbenzene m/z147.118 (30 %). Terpenes are used in the food & beverages, cosmetics, pharmaceutical, and rubber industry. In addition, this factor also explains the largest percentage share of a large suite of volatile and IVOC aromatic hydrocarbons including naphthalene m/z129.070 (42 %, $\log_{10}C_0$ 5.4), methyl naphthalene m/z143.086 (38 %, $\log_{10}C_0$ 5.3), $C_{12}H_{16}$ m/z161.134 (38 %, $\log_{10}C_0$ 5.4 to 6.3), $C_{13}H_{18}$ m/z175.150 (41 %, $\log_{10}C_0$ 4.9 to 5.6), $C_{13}H_{20}$ m/z177.165 (36 %, $\log_{10}C_0$ 5.4 to 5.8), $C_{13}H_{22}$ m/z179.181 (36 %, $\log_{10}C_0$ 5.2 to 6.4), $C_{14}H_{20}$ m/z189.165 (37.0 %, $\log_{10}C_0$ 4.8 to 5.1), and $C_{14}H_{22}$ m/z191.181 (34 %, $\log_{10}C_0$ 4.9 to 5.3). Ambient observations for most of these IVOCs have not been reported in the literature so far. Only, C_9H_{14}, $C_{12}H_{12}$ and $C_{12}H_{16}$ have been reported from aircraft engine emissions (Kılıç et al., 2018) while terpenes,

C_9H_{16}, cyclopentylbenzene, naphthalene and methyl naphthalene have been reported from a wide range of combustion sources (Hatch et al., 2015, Bruns et al., 2017). Most other compounds have so far only been reported to degas from heated asphalt (Khare et al., 2020). Due to the high abundance of IVOCs in this factor, it contributes 15 % to the total SOA formation potential.

3.2.8 Factor 8: Solvents and Evaporative Emissions

Solvent usage and evaporative emissions reach the site from several point sources and wind directions often in the form of short and intense plumes that show no correlation with combustion tracers. This source contributes most to the VOC burden at night and explains 6 % of the total VOC but ≤1 % of the total $PM_{2.5}$ & PM_{10} mass (Fig. 4). The source fingerprint of the solvents factor (Fig. 3) is characterized in descending rank of mass contribution by acetic acid + glycolaldehyde (4.7 μgm^{-3}), toluene (1.4 μgm^{-3}), methanol (0.8 μgm^{-3}), butanoic acid/ethyl acetate m/z89.058 (0.7 μgm^{-3}), acetone + propanal (0.5 μgm^{-3}) and butanal + butanone + MEK m/z73.062 (0.4 μgm^{-3}) and shows the greatest similarity to ambient air grab samples from Munirka furniture market and the dry cleaning shops at Dhobighat near Akshar Dham. Figure S3(c) shows that the factor explains the largest share of organic acids namely butanoic acid (52 %), acetic acid (41 %) and isocyanic acid m/z44.018 (25 %) and the second largest share of butanal + butanone + MEK (16 %). These compounds point towards chemical, food and pharmaceutical industries or polymer manufacturing as likely sources of these emissions.

3.2.9 Factor 9: Road construction

The road construction factor is almost absent during monsoon season, as road repair work is mostly avoided during this period due to water logging risks, and emissions from this source generally peak during the day as degassing of compounds from asphalt is temperature-driven and continues for days after the initial paving (Khare et al., 2020). The source fingerprint of the road construction factor is characterized in descending order of the mass concentrations by acetone + propionaldehyde (4.7 μgm^{-3}), toluene (1.7 μgm^{-3}), methanol (1.2 μgm^{-3}), benzene (0.7 μgm^{-3}) and C8-aromatics (0.7 μgm^{-3}). Acetone and propionaldehyde were found to be the most abundant compounds emitted during asphalt paving (Li et al., 2020). The source profile had the greatest similarity with the mix of emissions that would originate from asphalt paving (Li et. al., 2020) and the tailpipe of road construction vehicles (Che et. al., 2023). As represented by Fig. S3(d), this factor explains the largest percentage share of a large suite of volatile and IVOC hydrocarbons namely, heptene m/z99.116 (24 %), $C_{11}H_{12}$ m/z145.102 (27 %, $\log_{10}C_0$ 5.8 to 6.2), $C_{12}H_{12}$ m/z157.099 (32 %, $\log_{10}C_0$ 4.0 to 5.8), $C_{14}H_{14}$ m/z183.121 (42 %, $\log_{10}C_0$ 3.2 to 5.8), $C_{14}H_{18}$ m/z187.148 (38 %, $\log_{10}C_0$ 4.5 to 4.8), $C_{16}H_{24}$ m/z217.195 (37 %, $\log_{10}C_0$ 3.7 to 5.2), $C_{17}H_{28}$ m/z233.228 (43 %, $\log_{10}C_0$ 3.7 to 4.4), and $C_{18}H_{30}$ m/z247.243 (44 %, $\log_{10}C_0$ 2.3 to 5.0). In addition, it explains the second largest percentage share of many other IVOC hydrocarbons namely C_9H_{14} (25 %, $\log_{10}C_0$ 7.2 to 7.6), C_9H_{16} (24 %, $\log_{10}C_0$ 5.8 to 7.9), $C_{11}H_{14}$ (22 %, $\log_{10}C_0$ 5.9 to 6.2), $C_{12}H_{16}$ (23 %, $\log_{10}C_0$ 5.4-6.3), $C_{13}H_{18}$ (22 %, $\log_{10}C_0$ 4.9 to 5.6), $C_{13}H_{20}$ (28 %, $\log_{10}C_0$ 5.4 to 5.8), $C_{13}H_{22}$ (27 %, $\log_{10}C_0$ 5.2 to 6.4), $C_{14}H_{20}$ (31 %, $\log_{10}C_0$ 4.8 to 5.1), $C_{14}H_{22}$ (31 %, $\log_{10}C_0$ 4.9 to 5.3). Except for the four hydrocarbons C_7H_{14}, C_9H_{14}, C_9H_{16}, and $C_{11}H_{12}$, all of these IVOCs have been reported to degas at 60°C from asphalt pavement (Khare et al., 2020). So far only $C_{14}H_{18}$ has been reported as fresh gas phase emissions (transport time <2.5 min) from a farm (Loubet et al.,

https://doi.org/10.5194/egusphere-2024-501
Preprint. Discussion started: 23 February 2024

2022) in ambient air, while $C_{17}H_{28}$ has been reported in the aerosol phase (Xu et al., 2022). The road construction factor also explains the largest percentage share of a long list of OVOCs namely, C6 diketone isomers m/z115.075 (25 %), C2-substituted phenol m/z123.080 (22 %), $C_7H_{12}O_2$ m/z129.092 (29 %), $C_8H_{14}O_2$ m/z143.108 (31 %), $C_8H_{16}O_2$ m/z145.123 (26 %), phthalic anhydride ($C_8H_4O_3$) m/z149.024 (33 %), which is a naphthalene oxidation product (Bruns et al., 2017), $C_9H_{10}O$ m/z135.080 (22 %), $C_9H_{12}O_2$ m/z153.0916 (30 %), $C_9H_{14}O_2$ m/z155.108 (33 %), $C_9H_{16}O_2$ m/z157.122 (32 %), $C_9H_{18}O_2$ m/z159.140 (27 %), $C_{10}H_{12}O$ m/z149.096 (23 %), $C_{10}H_{18}O$ m/z155.144 (33 %), $C_{10}H_8O_3$ m/z177.056 (44 %), $C_{10}H_{16}O_3$ m/z185.121 (33 %), and $C_{12}H_{18}O_2$ m/z195.138 (41 %). However, out of these only $C_{10}H_{12}O$ and $C_{10}H_{18}O$ have been detected as direct emissions from heated asphalt pavement (Khare et al., 2020) indicating that most OVOCs in this factor are possibly oxidation products of short-lived IVOCs hydrocarbons emitted by this source.

3.2.10 Factor 10: Photochemistry

The photochemical factor has a diurnal profile that follows the diurnal profile of ozone (R=0.4). The factor profile is dominated by OVOCs such as acetic acid (1.9 µgm^{-3}), formic acid (1.2 µgm^{-3}) acetaldehyde (1.0 µgm^{-3}), formamide (0.3 µgm^{-3}), and methanol (0.3 µgm^{-3}). Figure S3(c) shows that the factor explains the largest percentage share of formic acid m/z47.009 (74.4 %), formamide m/z46.025 (73.3 %), and methyl glyoxal m/z73.026 (33.9 %). It also explains the second largest percentage share of isocyanic acid (19 %) and hexanamide (23 %), which are formed by the photooxidation of amines (Yao et al., 2016; Wang et al., 2022). Some compounds point towards a significant contribution of photochemically aged biomass burning emissions to this factor for example furfuryl alcohol (23 %), hydroxymethyl furanone (27 %), and hydroxybenzaldehyde m/z123.044 (22 %). While this factor explained ≤4 % of the total VOC share and negligible share of $PM_{2.5}$ and PM_{10} mass in Delhi, photochemically aged biomass burning emissions were a significant source of VOCs at a suburban site in Punjab during the post-monsoon season of 2017 (Singh et al., 2023). The difference is likely due to the fact that great smog episode of 2017 was primarily driven by low wind speeds a shallow boundary layer and regional-scale build-up of emissions over a prolonged period (Dekker et al., 2019, Roozitalab, et al., 2021), while the post-monsoon season of 2022 experienced western disturbances and higher ventilation coefficients. The factor also explains the largest percentage share of the total mass for organic acids such as nonanoic acid m/z159.14 (27 %), n-octanoic acid m/z145.123 (24 %) which have been detected in biomass-burning impacted environments in China (Mochizuki et al., 2019), $C_{12}H_{18}O_2$ (13 %) which has been found in aged wildfire plumes in the US (Haeri, 2023), and the terpene ozonolysis products norpinonaldehyde m/z155.108 (17 %) and cis-Pinonic acid m/z185.121 (23 %) (Camredon et al., 2010) and $C_7H_{12}O_2$ m/z129.092 (17 %). Pinonic acid was found to be an important aerosol phase tracer of biogenic SOA formation in India (Mahilang et al., 2021) and $C_7H_{12}O_2$ has been reported as a pinonic acid aqueous-phase photolysis product (Lignell et al., 2013) Fig. S3(c).

3.2.11 Factor 11: Biogenic

Biogenic VOC emissions at the receptor site show the highest cross-correlation with photosynthetic active radiation (PAR, R=0.7) and temperature (R=0.7) (Table S4) and explain 4 % of the total VOC burden and 2 % of the PM_{10} burden in the PMF.

https://doi.org/10.5194/egusphere-2024-501
Preprint. Discussion started: 23 February 2024

The BVOC emission in this factor is relatively fresh as the ratio of isoprene to its first-generation oxidation products MEK and MVK+MACR is 5.9 and 3.0 respectively. At the site, the top of the tree canopy of roadside trees is located approximately 20 m below the inlet height. Figure 3 shows that in descending rank of mass contribution, acetaldehyde m/z45.03 (1.2 µgm^{-3}), C_3H_4 m/z41.035 (1.1 µgm^{-3}), isoprene m/z69.067 (0.8 µgm^{-3}), acetic acid+glycolaldehyde m/z61.025 (0.6 µgm^{-3}) and acetone + propanal m/z59.046 (0.6 µgm^{-3}) are the major contributors for biogenic factor and that the source fingerprint showed the greatest similarity to a mix of BVOC emissions leaf wounding compounds (Portillo-Estrada et al., 2015) and BVOC emissions (Park et al., 2013). The signal at m/z41.035 can potentially be attributed to a 2-methyl-3-butene-2-ol fragment (Kim et al., 2010; Park et al., 2013). Figure S3(c) shows that this factor explains the largest percentage share of two BVOCs namely Isoprene + 2-methyl-3-butene-2-ol fragment m/z69.067 (34 %), and its oxidation product, methyl vinyl ketone, methacrolein and 2-butenal m/z71.047 (25 %). It also explains the largest percentage share of C-6 amides m/z116.108 (30 %) which are produced by the photo-oxidation of amines (Yao et al., 2016). The potential precursor, C6-amines have previously been detected in forested environments (You et al., 2014). However, it is also possible that C-6 amides are only attributed to the biogenic factor because their diurnal concentration profile matches that of first-generation oxidation products, and the source strength is high during both monsoon and post-monsoon season. This type of time series would also be expected if the precursors of this oxidation product are emitted from agricultural activities.

3.3. Comparison with emission inventories

The Figure 6 shows a comparison of different anthropogenic emission inventories with the PMF output data from this study for three overlapping fetch regions corresponding to different airflow patterns. We contrast emissions for the north-westerly flow with a fetch that includes Pakistan Punjab, Indian Punjab, Haryana, Western Uttar Pradesh, Himachal Pradesh, and Uttarakhand with air masses that arrive at the receptor from a south-westerly direction which carry emissions from southern Punjab, Haryana, Uttar Pradesh, Madhya Pradesh, Rajasthan and Gujarat, and air masses that reach the site from the south easterly direction which primarily carry emissions from Haryana, Southern Uttarakhand, Uttar Pradesh, Bihar and Nepal.

One feature that stands out in this comparison is that all inventories appear to significantly overestimate the relative contribution of residential fuel usage to the VOC and particulate matter emissions for all fetch regions. In absolute terms, the Regional Emission Inventory in Asia (REAS v3.2.1) for the year 2015 (Kurokawa & Ohara, 2020) and the Emission Database for Global Atmospheric Research (EDGARv6.1) for the year 2018 (Crippa et al., 2022), agree on the residential sector $PM_{2.5}$ emissions of 379 Gg y^{-1} and 382 Gg y^{-1}, respectively, for the NW fetch region. According to the latest estimates (Pandey et al., 2021), the NW-IGP region has the lowest prevalence of solid fuel usage in the entire IGP and the inventories appear to overestimate the $PM_{2.5}$ emissions from this fetch region only by a factor of 1.5-1.9. For the SW and SE fetch region, respectively, REAS v3.2.1 estimates much larger residential sector $PM_{2.5}$ emissions of 934 Gg y^{-1}, and 830 Gg y^{-1} than EDGARv6.1 (713 Gg y^{-1}, and 597 Gg y^{-1}) and overestimates the PMF estimates by a factor of 3.7 and 4.6. In contrast, EDGARv6.1 only overestimates PMF estimates by a factor of 1.8 and 3.2, for the SW and SE fetch region respectively. Solid fuel-based cooking is more prevalent in both Central and Western India and the Eastern IGP than in the NW-IGP (Pandey et

https://doi.org/10.5194/egusphere-2024-501
Preprint. Discussion started: 23 February 2024

al., 2021). The overestimation in both inventories may be caused by a gradual adoption of cleaner technology. Sharma et al., (2022) calculated a 13 % drop in residential sector $PM_{2.5}$ emissions between 2015 and 2020 due to higher LPG sales and a continuation of that trend to 2022 could explain the overestimation of residential fuel usage in the present emission inventory data. For PM_{10}, the EDGARv6.1 emission estimates of 750 Gg y^{-1}, 1391 Gg y^{-1}, and 1157 Gg y^{-1} for the NW, SW and SE fetch region, respectively, are greater than the REASv3.2.1 inventory estimates of 401 Gg y^{-1}, 994 Gg y^{-1}, and 882 Gg y^{-1}, for the NW, SW, and SE fetch region, respectively.

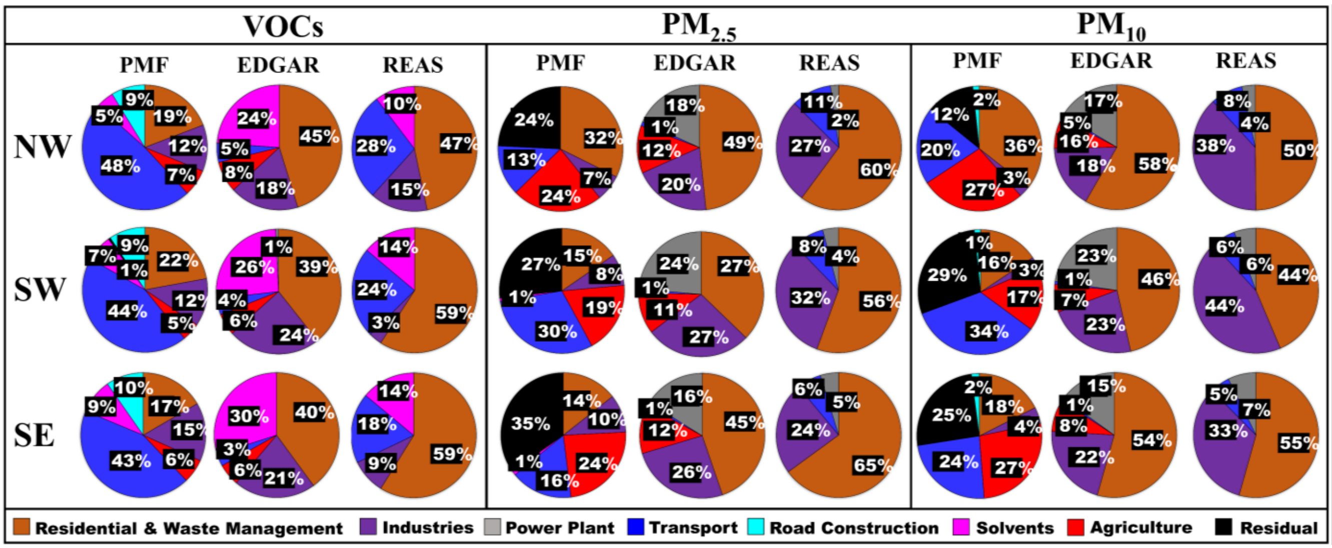

Figure 6: Comparison of different anthropogenic emission inventories with the PMF output from this study for three overlapping fetch regions corresponding to different airflow patterns.

The EDGARv6.1 and REASv3.2.1 inventory both overestimate our PMF PM_{10} results by a factor of 1.5 to 3.0. However, while the REASv3.2.1 inventory appears to assume that most of the residential sector aerosol emissions occur in the fine mode, our PMF results (Fig. 6) clearly agree with the EDGARv6.1 inventory on the fact that there are significant coarse aerosol emissions associated with solid-fuel based cooking and heating. For VOCs the EDGARv6.1 emission estimates of 764 Gg y^{-1}, 1421 Gg y^{-1}, and 1196 Gg y^{-1}, for the NW, SW, and SE fetch region, respectively, are almost twice as large as the REASv3.2.1 inventory estimates of 353 Gg y^{-1}, 947 Gg y^{-1}, and 862 Gg y^{-1}, even though the percentage contribution of this sector to the VOC burden appears to be similar for both. The cause of this are the larger VOC emissions from solvent use and industries in the EDGARv6.1 inventory. Both inventories overestimate our PMF-based estimate by more than a factor of two.

With respect to industrial emissions of VOCs for the NW fetch region, our PMF results indicate that the actual emissions are slightly smaller than those in the REASv3.2.1 inventory (113 Gg y^{-1}), while the EDGARv6.1 inventory (302 Gg y^{-1}) overestimates emissions. For the SW and SE fetch region, our PMF estimates fall in between those of the EDGARv6.1 inventory (867 Gg y^{-1}, and 635 Gg y^{-1}) and the REASv3.2.1 inventory (55 Gg y^{-1}, and 133 Gg y^{-1}). For industrial $PM_{2.5}$

https://doi.org/10.5194/egusphere-2024-501
Preprint. Discussion started: 23 February 2024

emissions, both EDGARv6.1 & REASv3.2.1 are close and agree on the magnitude of emissions of 158 & 173 Gg y^{-1}, 524 & 541 Gg y^{-1}, and 342 & 307 Gg y^{-1} for the NW, SW and SE fetch region, respectively, and both inventories appear to overestimate emissions when compared to our PMF results. Our findings seem to suggest that the pollution boards have been somewhat successful in clamping down on industrial emissions and the technology employed is better than what is currently reflected in emission inventories. Industrial fly ash (PM_{10}) emissions are larger in the REASv3.2.1 inventory (308 Gg y^{-1}, 1015 Gg y^{-1}, and 539 Gg y^{-1} for the NW, SW and SE fetch region, respectively) compared to EDGARv6.1 inventory (211 Gg y^{-1}, 684 Gg y^{-1}, and 458 Gg y^{-1} for the NW, SW and SE fetch region, respectively). Yet both inventories appear to significantly overestimate industrial emissions when compared to our PMF results. These findings also indicate the pollution boards have been somewhat successful in clamping down on large and visible fly ash sources and that the EDGARv6.1 inventory has captured this clean-technology transition better.

The REASv3.2.1 inventory completely misses direct VOC and PM emissions from the agricultural sector. In contrast, the EDGARv6.1 inventory significantly underestimates $PM_{2.5}$ & PM_{10} emissions from agricultural activities, which include, but are not limited to crop residue burning, in comparison to our PMF results. The EDGARv6.1 inventory attributes 97 & 103 Gg y^{-1}, 206 & 217 Gg y^{-1}, and 168 & 177 Gg y^{-1} of $PM_{2.5}$ & PM_{10} emissions, for the NW, SW, and SE fetch region respectively, to agricultural activities for the full year. This stands in stark contrast to the FINNv2.5 inventory (Wiedinmyer et al., 2023), which attributes 192 & 95 Gg y^{-1}, 203 & 100 Gg y^{-1}, and 52 & 26 Gg y^{-1} for the NW, SW, and SE fetch region, respectively, just to agricultural residue burning activities taking place between 15th and August and 26th November 2021 alone. The fact that EDGAR appears to underestimate residue-burning emissions has been flagged earlier (Pallavi et al., 2019; Kumar et al., 2021; Singh et al., 2023). Our PMF reveals that to agricultural residue burning emissions over the NW and SE fetch regions are comparable yet the order of magnitude of emissions over the SE fetch region is underestimated due to poor fire detection.

Transport sector VOC emissions appear to be severely underestimated in the EDGARv6.1 inventory which attributes 84 Gg y^{-1}, 154 Gg y^{-1}, and 96 Gg y^{-1} for the NW, SW, and SE fetch region, respectively, to this activity. This underestimation of transport sector emissions in the EDGAR inventory has been previously flagged for earlier versions of the same inventory (Sarkar et al., 2017; Pallavi et al., 2019; Singh et al., 2023). The REASv3.2.1 inventory attributes 212 Gg y^{-1}, 378 Gg y^{-1}, and 266 Gg y^{-1} VOC emission to the transport sector for the NW, SW, and SE fetch region, respectively. Both inventories underestimate our PMF results. This indicates that the contribution of the transport sector to ambient VOC pollution levels in a megacity like Delhi may not be adequately reflected in emission inventories. Our PMF suggests that the overall contribution of the transport sector to the total $PM_{2.5}$ and PM_{10} pollution levels occurs primarily due to non-exhaust emissions from the CNG-fuelled public transport fleet. These non-exhaust emissions are much larger than what is accounted for both in the EDGARv6.1estimate of 8 & 10 Gg y^{-1}, 18 & 22 Gg y^{-1}, and 12 & 14 Gg y^{-1} and the REASv3.2.1 estimate of 65 & 67 Gg y^{-1}, 137 & 140 Gg y^{-1}, and 80 & 83 Gg y^{-1} for $PM_{2.5}$ & PM_{10} emissions from the NW, SW and SE fetch region, respectively. The transport sector-related findings of this PMF source apportionment study are in agreement with earlier source apportionment studies that often attributed a quarter or more of the total PM emissions to the transport sector. Some prior studies used metals, Pb and/or OC/EC as transport sector activity tracers (Jain et al., 2017, 2020; Sharma et al., 2016, Jaiprakash et al., 2016;

https://doi.org/10.5194/egusphere-2024-501
Preprint. Discussion started: 23 February 2024

Sharma & Mandal, 2017), while others attributed almost the entire HOA component of organic aerosol to transport sector emissions (Reyes-Villega et al., 2021; Cash et al., 2021; Kumar et al., 2022, Shukla et al., 2023) or used a Chemical Mass Balance (CMB) model with source fingerprints from the EPA database (Nagar et al., 2017). Our PMF results differ to emission-inventory-based assessments, which only attribute a minor share of the total PM burden to this activity (Guo et al., 2017). Our findings also add dimension to the reasons why the transport sector targeted air quality interventions yielded such poor results (Chandra et al., 2018). Public transport availability was ramped up during the periods when road-rationing schemes restricted the use of private 4-wheelers. Our results suggest that only investments into the road infrastructure, that reduce resuspension, modal shifts from buses towards metro-based public transport and electric vehicles with >50 % regenerative braking (Liu et al., 2021) that limit brake wear can yield meaningful reductions in the transport sector-related PM emissions.

Our PMF results indicate that solvent usage results in VOC emissions that are more in line with the REASv3.2.1 inventory which estimates emissions of 78 Gg y^{-1}, 222 Gg y^{-1}, and 204 Gg y^{-1} from the NW, SW and SE fetch region, respectively. The EDGARv6.1 inventory attributes 403 Gg y^{-1}, 939 Gg y^{-1}, and 896 Gg y^{-1}, to solvent usage emissions from the NW, SW and SE fetch region, respectively and overestimates emissions by a factor of 4.

Power generation is not considered to be a significant VOC source in both emission inventories (<27 Gg y^{-1} and <1 % of the total VOC mass), and fails to show up as a separate sector in our PMF results, as our model runs rely on VOC tracers to track pollution sources. The contribution of energy generation towards the PM burden particularly in the EDGARv6.1 emission inventory, however, is significant. The sector contributes 144 & 212 Gg y^{-1}, 453 & 679 Gg y^{-1}, and 215 & 321 Gg y^{-1} of $PM_{2.5}$ and PM_{10} emissions, for the NW, SW, and SE fetch regions, respectively. It is, however, striking to note that the PMF features a residual that is of similar magnitude as the $PM_{2.5}$ and PM_{10} emissions attributed to power generation in the EDGARv6.1 inventory. Power generation is believed to primarily contribute secondary sulfate and nitrate aerosol (Atabakhsh et. al., 2023), which is unlikely to be directly associated with a fresh combustion signature. It is hence likely, that much of our PMF residual can be attributed primarily to this source. The amount of emissions attributed to power generation in the REASv3.2.1 inventory is much smaller than those reflected in EDGARv6.1, likely because the inventories miss several coal generation units that were commissioned between 2015-2018.

Our PMF results identify road construction and asphalt pavements as an additional VOC source that is at present not reflected in emission inventories.

4 Conclusions

This study presents source-apportionment results derived from application of the positive matrix factorization model to a recently acquired high-quality dataset of $PM_{2.5}$ & PM_{10}, and 111 VOCs measured using the new PTR-TOF-MS10K enhanced volatility instrument, during monsoon and post-monsoon seasons of 2022, from one world's most polluted megacities: Delhi. We found that the top ranked major emission source of gas phase and aerosol phase differed from each other, highlighting the

https://doi.org/10.5194/egusphere-2024-501
Preprint. Discussion started: 23 February 2024

complexity of air pollution sources in such atmospheric environments. While fresh paddy burning was a negligible source of VOCs (6 %), it was the largest source of $PM_{2.5}$ & PM_{10} (23 % & 25 %) in the Delhi NCR regions during our study period, the two criteria air pollutants that are thought to be the leading cause of the air pollution emergency in November in Delhi annually (Khan et. al., 2023). The strong correlation of $PM_{2.5}$ & PM_{10} with same-day fire counts, and VOC emission signatures of fresh paddy burning plumes showed that fires burning in and within the vicinity of Delhi-NCR and plumes that reached the receptor on the same day were the stronger contributory source of the high pollution levels, compared to plumes from more distant states such as Punjab and Pakistan Punjab. Both are located north-west of Delhi-NCR and were thought to be the stronger contributors to the pollution levels because the detected fire activity is more prevalent there. Furthermore, $PM_{2.5}$ & PM_{10} emissions from residential heating and waste disposal (24 % & 23 %) rival those from crop residues burning and unlike paddy residue burning emissions, which are episodic, this activity persists into winter. While popular perception generally blames burning in Punjab for the high particulate matter burden due to paddy stubble burning, our PMF reveals that despite the much lower fire counts over the Eastern IGP (17,810) when compared to the North Western IGP (61,334) both are a significant source of paddy stubble burning PM in the NCR region. Also, sources that are generally targeted by most clean air action plans such as tailpipe exhaust emissions of private vehicles and industries are responsible for less than one-quarter of the particulate matter mass loading that can be traced with the help of gas-phase organic molecular tracers. Instead, the transport sector's PM emissions are dominated by the non-exhaust emissions of the CNG-fueled commercial vehicle fleet.

The PMF results based on primary in-situ data indicate that the EDGARv6.1 inventory provides a better representation of emissions for most sectors, with the exception of agricultural residue burning emissions, the transport sector and VOC emissions from solvent use. At present none of the residential sector inventories appears to have incorporated the change in the magnitude and spatial patterns due to the recent adoption of cleaner cooking technology interventions since 2018. Transport sector non-exhaust emissions are still absent (REASv3.2) or underestimated (EDGARv6.1) in all inventories, whereas agricultural residue burning emissions over the Delhi-NCR region are best represented by the FINNv2.5 inventory (Wiedinmyer et al., 2023). For VOC emissions from solvent usage, REASv3.2 provides better emissions than EDGARv6.1. There is also a road construction sector in our PMF results which has a significant (9-10 %) contribution to the VOC burden but hasn't been addressed in any of the emission inventories so far, and our study by including measurements of specific molecular markers of this activity has been able to shed new strategic insights concerning this missing source.

A considerable portion of the PM_{10} (18 %) and $PM_{2.5}$ (28 %) load is connected to residual sources, not directly related to combustion tracers. This contribution is likely due to windblown dust transported over long distances as well as secondary inorganic aerosols like ammonium sulfate and ammonium nitrate whose precursors are primarily emitted from power plants. Despite including the most, comprehensive set of organic species to date, our study does not include similar information about these other species. Residential heating and waste disposal were identified as one of the largest contributors to PM pollution and are active year-round with strengths varying depending on seasonality. So, targeting these through improved access to cleaner energy sources for heating and cooking would likely improve air quality significantly in other seasons. Future similarly designed quantitative studies would be needed to confirm this hypothesis.

https://doi.org/10.5194/egusphere-2024-501
Preprint. Discussion started: 23 February 2024

The findings and insights from this study emphasize the necessity for a comprehensive, multi-sectoral approach to reduce primary emissions. While several recent efforts in some sectors (e.g. residential biofuel and cooking) appear to have yielded emission reduction benefits, the narrative to blame the pollution at this time of the year on the more visible sources (e.g. paddy residue burning) needs to be corrected so other sources are also mitigated. Our findings support the assertions of (Ganguly et al., 2020), who have pointed out previously that rather than solely focusing on specific sources like agricultural residue burning or transport emissions, it's crucial to address the disparity between the primary targets of clean air action plans and the actual dominant sources of particulate matter. Future action plans need to account for more targeted and impactful pollution control measures and also a more comprehensive approach to address the diverse urban mixed sources highlighted in this study, such as industries and residential solid fuel/waste burning, non-exhaust road emissions, and emissions from road construction.

This new approach of combining VOC tracers with PM measurements provides great potential for improved source apportionment in complex emission environments, at a level of detail that is more meaningful than just attributing emissions to biomass burning or fossil-fuel burning, which has been the case in all previous studies from the region till date. The study design which captured contrasts between clean-monsoon and polluted-post-monsoon air, and included measured VOC source fingerprints and molecular tracers enabled us to distinguish paddy-residue burning from other biomass burning sources, and resolve similar traffic emission sources (e.g. 2-wheelers from 4-wheelers and CNG vehicles). This provides a significant advance over existing source-apportionment studies and its application would be of great relevance in other complex emission environments suffering from high air pollution where quantitative knowledge of sources can lead to evidence-based emission reduction prioritization efforts and a better understanding of the atmospheric chemistry of polluted environments around the world.

Data availability

PMF model simulations and input data can be obtained by contacting Baerbel Sinha.

Author Contribution

Arpit Awasthi: Data curation, Formal analysis, Investigation, Software, Visualization, Writing – original draft preparation. Baerbel Sinha: Conceptualization, Data curation, Formal analysis, Methodology, Project administration, Resources, Software, Supervision, Validation, review & editing, Writing – review & editing. Haseeb Hakkim: Data curation, Formal analysis, Investigation, Writing – review & editing. Sachin Mishra: Data curation, Formal analysis, Investigation. Varkrishna M.: Investigation. Gurmanjot Singh: Investigation. Sachin D. Ghude: Resources. Vijay Kumar Soni: Resources. N. Nigam: Resources. Vinayak Sinha: Conceptualization, Data curation, Project administration, Methodology, Supervision, Writing – review & editing. M. Rajeevan: Resources.

Competing Interests

The authors declare that they have no conflict of interest.

Acknowledgements:

We acknowledge the financial support given by the Ministry of Earth Sciences (MOEs), the government of India, to support the RASAGAM (Realtime Ambient Source Apportionment of Gases and Aerosol for Mitigation) project at IISER Mohali vide grant MOES/16/06/2018-RDEAS Dt. 22.6.2021. S.M acknowledges IISER Mohali for Institute PhD fellowship. AA acknowledges MoE for PMRF PhD fellowship. We thank Dr. R. Mahesh, Dr. Gopal Iyengar, Dr. R. Krishnan (Director, IITM Pune), Prof. Gowrishankar (Director, IISER Mohali), Dr. M. Mohapatra (DG, IMD), Dr. M. Ravichandran (Secretary Ministry of Earth Science) for their encouragement and support. We thank student members of the Atmospheric Chemistry and Emissions (ACE) research group and Aerosol Research Group (ARG) of IISER Mohali and IITM Pune in particular AkashVispute and PrassanaLonkar and local scientists of IMD for their local logistics support. The authors gratefully acknowledge the NASA/ NOAA Suomi National Polar-orbiting Partnership (Suomi NPP) and NOAA-20 satellites VIIRS fire count data used in this publication. The authors gratefully acknowledge the NOAA Air Resources Laboratory (ARL) for the provision of the HYSPLIT transport and dispersion model used in this publication.

References

Achten, C., Kolb, A., and Püttmann, W.: Methyl tert-butyl ether (MTBE) in urban and rural precipitation in Germany. Atmos. Environ., 35(36), 6337-6345, https://doi.org/10.1016/S1352-2310(01)00423-X, 2001.

Acharja, P., Ali, K., Ghude, S. D., Sinha, V., Sinha, B., Kulkarni, R., Gultepe, I., Rajeevan, M. N.: Enhanced secondary aerosol formation driven by excess ammonia during fog episodes in Delhi, India, Chemosphere 289, 133155, https://doi.org/10.1016/j.chemosphere.2021.133155, 2022.

Atabakhsh, S., Poulain, L., Chen, G., Canonaco, F., Prévôt, A. S. H., Pöhlker, M., Wiedensohler, A., and Herrmann, H.: A 1-year aerosol chemical speciation monitor (ACSM) source analysis of organic aerosol particle contributions from anthropogenic sources after long-range transport at the TROPOS research station Melpitz, Atmos. Chem. Phys., 23, 6963–6988, https://doi.org/10.5194/acp-23-6963-2023, 2023.

Bow, S.-T.: Pattern Recognition, Application to Large Data Set Problems, Marcel Dekker, Inc., 1984. 12. Therrien, C. W., Decision, Estimation and Classification, An Introduction to Pattern Recognition and Related Topics, John Wiley and Sons, https://ui.adsabs.harvard.edu/abs/1984prat.book.....B, 1984.

Bruns, E. A., Slowik, J. G., El Haddad, I., Kilic, D., Klein, F., Dommen, J., Temime-Roussel, B., Marchand, N., Baltensperger, U., and Prévôt, A. S. H.: Characterization of gas-phase organics using proton transfer reaction time-of-flight mass spectrometry: Fresh and aged residential wood combustion emissions, Atmos. Chem. Phys., 17(1), 705–720, https://doi.org/10.5194/acp-17-705-2017, 2017.

Camredon, M., Hamilton, J. F., Alam, M. S., Wyche, K. P., Carr, T., White, I. R., Monks, P. S., Rickard, A. R., and Bloss, W. J.: Distribution of gaseous and particulate organic composition during dark α-pinene ozonolysis, Atmos. Chem. Phys., 10, 2893–2917, https://doi.org/10.5194/acp-10-2893-2010, 2010.

Carslaw, D. C. and Ropkins, K.: openair – An R package for air quality data analysis, Environ. Modell. Softw., 27–28, 52–61, https://doi.org/10.1016/j.envsoft.2011.09.008, 2012.

Carter, W. P. L.: Updated maximum incremental reactivity scale and hydrocarbon bin reactivities for regulatory applications, prepared for California Air Resources Board Contract 07-339, available at: http://cmscert.engr.ucr.edu/~carter/SAPRC/MIR10.pdf (last access: July 2018), 2000.

Cash, J. M., Langford, B., Di Marco, C., Mullinger, N. J., Allan, J., Reyes-Villegas, E., Joshi, R., Heal, M. R., Acton, W. J. F., Hewitt, C. N., Misztal, P. K., Drysdale, W., Mandal, T. K., Shivani, Gadi, R., Gurjar, B. R., and Nemitz, E.: Seasonal analysis of submicron aerosol in Old Delhi using high-resolution aerosol mass spectrometry: chemical characterisation, source apportionment and new marker identification, Atmos. Chem. Phys., 21, 10133–10158, https://doi.org/10.5194/acp-21-10133-2021, 2021.

Chandra, B. P., and Sinha, V.: Contribution of post-harvest agricultural paddy residue fires in the N.W. Indo-Gangetic Plain to ambient carcinogenic benzenoids, toxic isocyanic acid and carbon monoxide. Environ. Int., 88, 187–197, https://doi.org/10.1016/J.ENVINT.2015.12.025, 2016.

Chandra, B. P., Sinha, V., Hakkim, H., and Sinha, B.: Storage stability studies and field application of low-cost glass flasks for analyses of thirteen ambient VOCs using proton transfer reaction mass spectrometry. Int. J. Mass. Spectrom., 419, 11-19, https://doi.org/10.1016/j.ijms.2017.05.008, 2017.

Chandra, B. P., Sinha, V., Hakkim, H., Kumar, A., Pawar, H., Mishra, A. K., Sharma, G., Pallavi, Garg, S., Ghude, S. D., Chate, D. M., Pithani, P., Kulkarni, R., Jenamani, R. K. and Rajeevan M.: Odd–even traffic rule implementation during winter 2016 in Delhi did not reduce traffic emissions of VOCs, carbon dioxide, methane and carbon monoxide. Curr. Sci. India., Vol. 114, 1318-1325, https://www.jstor.org/stable/26797338, 2018.

Chaudhary, P., Garg, S., George, T., Shabin, M., Saha, S., Subodh, S., Sinha, B.: Underreporting and open burning–the two largest challenges for sustainable waste management in India. Resour. Conserv. Recycl. 175, 105865, https://doi.org/10.1016/j.resconrec.2021.105865, 2021.

Chaudhary, P., Singh, R., Shabin, M., Sharma, A., Bhatt, S., Sinha, V., and Sinha, B.: Replacing the greater evil: Can legalizing decentralized waste burning in improved devices reduce waste burning emissions for improved air quality? Environ. Pollut., 311, 119897, https://doi.org/10.1016/J.ENVPOL.2022.119897, 2022.

Che, H., Shen, X., Yao, Z., Wua, B., Gou, R., Hao, X., Cao, X., Li, X., Zhang, Z., Wang, S. and Chen, Z.: Real-world emission characteristics and inventory of volatile organic compounds originating from construction and agricultural machinery. Sci. Total. Environ. 894, 164993, https://doi.org/10.1016/j.scitotenv.2023.164993, 2023.

https://doi.org/10.5194/egusphere-2024-501
Preprint. Discussion started: 23 February 2024

Crippa, M., Guizzardi, D., Muntean, M., and Schaaf, E.: EDGAR v5.0 Global Air Pollutant Emissions, European Commission, Joint Research Centre (JRC) [data set], http://data.europa.eu/89h/377801af-b094-4943-8fdc-f79a7c0c2d19 (last access: 2 April 2020), 2019a.

Coggon, M. M., Lim, C. Y., Koss, A. R., Sekimoto, K., Yuan, B., Gilman, J. B., Hagan, D. H., Selimovic, V., Zarzana, K. J., Brown, S. S., M Roberts, J., Müller, M., Yokelson, R., Wisthaler, A., Krechmer, J. E., Jimenez, J. L., Cappa, C., Kroll, J. H., De Gouw, J., and Warneke, C.: OH chemistry of non-methane organic gases (NMOGs) emitted from laboratory and ambient biomass burning smoke: Evaluating the influence of furans and oxygenated aromatics on ozone and secondary NMOG formation. Atmos. Chem. Phys., 19(23), 14875–14899, https://doi.org/10.5194/ACP-19-14875-2019, 2019.

Datta, S., Sharma, A., Parkar, V., Hakkim, H., Kumar, A., Chauhan, A., Tomar S. S., and Sinha, B.: A new index to assess the air quality impact of urban tree plantation. Urban Climate 40 (2021) 100995, https://doi.org/10.1016/j.uclim.2021.100995, 2021.

Dekker, I.N., Houweling, S., Pandey, S., Krol, M., R¨ockmann, T., Borsdorff, T., Landgraf, J., and Aben, I.,: What caused the extreme CO concentrations during the 2017 high pollution episode in India? Atmos. Chem. Phys. 19, 3433–3445. https://doi.org/10.5194/acp-19-3433-2019, 2019.

Derwent, R. G., Jenkin, M. E., Saunders, S. M., and Pilling, M. J.: Photochemical ozone creation potentials for organic compounds in northwest Europe calculated with a master chemical mechanism, Atmos. Environ., 32(14–15), 2429–2441, https://doi.org/10.1016/S1352-2310(98)00053-3, 1998.

Derwent, R. G., Jenkin, M. E., Utembe, S. R., Shallcross, D. E., Murrells, T. P., and Passant, N. R.: Secondary organic aerosol formation from a large number of reactive man-made organic compounds. Sci. Total. Environ., 408(16), 3374–3381, https://doi.org/10.1016/J.SCITOTENV.2010.04.013, 2010.

Fadly, D., Fontes, F., and Maertens, M.: Fuel for food: Access to clean cooking fuel and Food Secur in India. Food Secur, 15(2), 301-321, https://doi.org/10.1007/s12571-023-01350-y, 2023.

Fleming, L. T., Weltman, R., Yadav, A., Edwards, R. D., Arora, N. K., Pillarisetti, A., Meinardi, S., Smith, K. R., Blake, D. R., and Nizkorodov, S. A.: Emissions from village cookstoves in Haryana, India, and their potential impacts on air quality, Atmos. Chem. Phys., 18, 15169–15182, https://doi.org/10.5194/acp-18-15169-2018, 2018.

Gajbhiye, M. D., Lakshmanan, S., Aggarwal, R., Kumar, N., and Bhattacharya, S.: Evolution and mitigation of vehicular emissions due to India's Bharat Stage Emission Standards–A case study from Delhi. Environmental Development, 45, 100803, https://doi.org/10.1016/j.envdev.2023.100803, 2023.

Ganguly, T., Selvaraj, K. L. and Guttikunda, S. K. National Clean Air Programme (NCAP) for Indian cities: Review and outlook of clean air action plans. Atmos. Environ.: X, 8, 100096, https://doi.org/10.1016/j.aeaoa.2020.100096, 2020.

Guo, H., Kota, S. H., Sahu, S. K., Hu, J., Ying, Q., Gao, A., and Zhang, H.: Source apportionment of PM2.5 in North India using source-oriented air quality models, Atmos. Chem. Phys., 17(1), 426-436, https://doi.org/10.1016/j.envpol.2017.08.016, 2017.

https://doi.org/10.5194/egusphere-2024-501
Preprint. Discussion started: 23 February 2024

Haeri, F.: Molecular Speciation of Organic Nitrogen Compounds Separated in Smoke Particles Emitted from Burning Western U.S. Wildland Fuels, PhD thesis, Carnegie Mellon University, Pittsburgh, PA, USA, https://doi.org/10.1184/R1/22670578.v1, 2023.

Hakkim, H., Kumar, A., Annadate, S., Sinha, B., and Sinha, V.: Air pollution scenario analyses of fleet replacement strategies to accomplish reductions in criteria air pollutants and 74 VOCs over India. Atmos. Environ.: X, 13, 100150, https://doi.org/10.1016/j.aeaoa.2022.100150, 2021.

Harrison, M. A. J., Heal, M. R., and Cape, J. N.: Evaluation of the pathways of tropospheric nitrophenol formation from benzene and phenol using a multiphase model. Atmos. Chem. Phys., 5, https://doi.org/10.5194/acp-5-1679-2005, 2022.

Harrison, M. A., Barra, S., Borghesi, D., Vione, D., Arsene, C., and Olariu, R. I.; Nitrated phenols in the atmosphere: a review. Atmos. Environ., 39(2), 231-248, https://doi.org/10.1016/j.atmosenv.2004.09.044, 2005.

Hatch, L. E., Luo, W., Pankow, J. F., Yokelson, R. J., Stockwell, C. E., and Barsant K. C.: Identification and quantification of gaseous organic compounds emitted from biomass burning using two-dimensional gas chromatography–time-of-flight mass spectrometry. Atmos. Chem. Phys., 15, 1865–1899, https://doi.org/10.5194/acp-15-1865-2015, 2015.

Hatch, L. E., Yokelson, R. J., Stockwell, C. E., Veres, P. R., Simpson, I. J., Blake, D. R., Orlando, J. J., and Barsanti K. C.: Multi-instrument comparison and compilation of non-methane organic gas emissions from biomass burning and implications for smoke-derived secondary organic aerosol precursors. Atmos. Chem. Phys., 17, 1471–1489, https://doi.org/10.5194/acp-17-1471-2017, 2017.

Hersbach, H., Bell, B., Berrisford, P., Biavati, G., Horányi, A., Muñoz Sabater, J., Nicolas, J., Peubey, C., Radu, R., Rozum, I., Schepers, D., Simmons, A., Soci, C., Dee, D., Thépaut, J-N.: ERA5 hourly data on single levels from 1940 to present. Copernicus Climate Change Service (C3S) Climate Data Store (CDS), https://doi.org/10.24381/cds.adbb2d47, 2023

Jain, S., Sharma, S. K., Choudhary, N., Masiwal, R., Saxena, M., Sharma, A., Mandal, T. K., Gupta, A., Gupta, N. C., and Sharma, C.: Chemical characteristics and source apportionment of PM2.5 using PCA/APCS, UNMIX, and PMF at an urban site of Delhi, India. Environ. Sci. Pollut. R., 24(17), 14637–14656, https://doi.org/10.1007/s11356-017-8925-5, 2017.

Jain, V., Tripathi, S.N., Tripathi, N., Sahu, L.K., Gaddamidi, S., Shukla, A.K., Bhattu, D., Ganguly, D.: Seasonal variability and source apportionment of non-methane VOCs using PTR-TOF-MS measurements in Delhi, India, Atmos. Environ. 283, 119163, https://doi.org/10.1016/j.atmosenv.2022.119163, 2022.

Jain, S., Sharma, S. K., Vijayan, N., and Mandal, T. K.: Seasonal characteristics of aerosols ($PM_{2.5}$ and PM_{10}) and their source apportionment using PMF: A four-year study over Delhi, India. Environ. Pollut., 262, https://doi.org/10.1016/j.envpol.2020.114337, 2020.

Jaiprakash, Singhai, A., Habib, G., Sunder Raman, R. and Gupta, T.: Chemical characterization of PM1.0 aerosol in Delhi and source apportionment using positive matrix factorization. Environ. Sci. Pollut. R., 24(45–462), https://doi.org/10.1007/s11356-016-7708-8, 2016.

Khan, A. A., Garsa, K., Jindal, P., and Devara, P. C. S.: Effects of stubble burning and firecrackers on the air quality of Delhi. Environ. Monit Assess., 195(10), 1170, https://doi.org/10.1007/s10661-023-11635-6, 2023.

Khare, P., Machesky, J., Soto, R. He, M., Presto, A. A. and Gentner, D. R.: Asphalt-related emissions are a major missing nontraditional source of secondary organic aerosol precursors. Science Advances, 6, eabb9785, https://doi.org/10.1126/sciadv.abb9785, 2020.

Kılıç, D., El Haddad, I., Brem, B. T., Bruns, E., Bozetti, C., Corbin, J., Durdina, L., Huang, R.-J., Jiang, J., Klein, F., Lavi, A., Pieber, S. M., Rindlisbacher, T., Rudich, Y., Slowik, J. G., Wang, J., Baltensperger, U., and Prévôt, A. S. H.: Identification of secondary aerosol precursors emitted by an aircraft turbofan. Atmos. Chem. Phys., 18, 7379–7391, https://doi.org/10.5194/acp-18-7379-2018, 2018.

Kim, S., Karl, T., Guenther, A., Tyndall, G., Orlando, J., Harley, P., Rasmussen, R., and Apel, E.: Emissions and ambient distributions of Biogenic Volatile Organic Compounds (BVOC) in a ponderosa pine ecosystem: interpretation of PTR-MS mass spectra. Atmos. Chem. Phys. 10, 1759–1771, https://doi.org/10.5194/acp-10-1759-2010, 2010.

Koss, A. R., Sekimoto, K., Gilman, J. B., Selimovic, V., Coggon, M. M., Zarzana, K. J., Yuan, B., Lerner, B. M., Brown, S. S., Jimenez, J. L., Krechmer, J., Roberts, J. M., Warneke, C., Yokelson, R. J., and De Gouw, J.: Non-methane organic gas emissions from biomass burning: Identification, quantification, and emission factors from PTR-ToF during the FIREX 2016 laboratory experiment. Atmos. Chem. Phys. 18(5), 3299–3319, https://doi.org/10.5194/ACP-18-3299-2018, 2018.

Kulkarni, S. H., Ghude, S. D., Jena, C., Karumuri, R. K., Sinha, B., Sinha, V., Kumar, R., Soni, V. K., and Khare M.: How Much Does Large-Scale Crop Residue Burning Affect the Air Quality in Delhi? Environ. Sci. Technol. 2020, 54, 4790−4799. https://doi.org/10.1021/acs.est.0c00329, 2020.

Kumar, V., Sarkar, C., and Sinha, V.: Influence of post-harvest crop residue fires on surface ozone mixing ratios in the NW IGP analyzed using 2 years of continuous in situ trace gas measurements, J. Geophys. Res.-Atmos., 121, 3619–3633, https://doi.org/10.1002/2015JD024308, 2016.

Kumar, A., Sinha, V., Shabin, M., Hakkim, H., Bonsang, B., and Gros, V.: Non-methane hydrocarbon (NMHC) fingerprints of major urban and agricultural emission sources for use in source apportionment studies. Atmos. Chem. Phys. 20(20), 12133–12152, https://doi.org/10.5194/ACP-20-12133-2020, 2020.

Kumar, A., Hakkim, H., Sinha, B., and Sinha, V.: Gridded 1 km × 1 km emission inventory for paddy stubble burning emissions over north-west India constrained by measured emission factors of 77 VOCs and district-wise crop yield data. Sci. Total. Environ., 789, 148064, https://doi.org/10.1016/J.SCITOTENV.2021.148064, 2021.

Kumar, V., Giannoukos, S., Haslett, S. L., Tong, Y., Singh, A., Bertrand, A., Lee, C. P., Wang, D. S., Bhattu, D., Stefenelli, G., Dave, J. S., Puthussery, J. V., Qi, L., Vats, P., Rai, P., Casotto, R., Satish, R., Mishra, S., Pospisilova, V., … Slowik, J. G.: Highly time-resolved chemical speciation and source apportionment of organic aerosol components in Delhi, India, using extractive electrospray ionization mass spectrometry Atmos. Chem. Phys. 22(11), 7739–7761, https://doi.org/10.5194/acp-22-7739-2022, 2022.

Kurokawa, J., and Ohara, T.: Long-term historical trends in air pollutant emissions in Asia: Regional Emission inventory in ASia (REAS) version 3. Atmos. Chem. Phys. 20(21), 12761–12793, https://doi.org/10.5194/ACP-20-12761-2020, 2020.

https://doi.org/10.5194/egusphere-2024-501
Preprint. Discussion started: 23 February 2024

Li, N., Jiang, Q., Wang, F., Xie, J., Li, Y., Li, J., and Wu, S.: Emission behaviour, environmental impact and priority-controlled pollutants assessment of volatile organic compounds (VOCs) during asphalt pavement construction based on laboratory experiment. J. Hazard. Mater. 398, 122904, https://doi.org/10.1016/j.jhazmat.2020.122904, 2020.

Li, Y., Pöschl, U., and Shiraiwa, M.: Molecular corridors and parameterizations of volatility in the chemical evolution of organic aerosols. Atmos. Chem. Phys. 16, 3327–3344, https:// https://doi.org/10.5194/acp-16-3327-2016, 2016.

Lignell, H., Epstein, S. A., Marvin, M. R., Shemesh, D., Gerber, B., and Nizkorodov, S.: Experimental and Theoretical Study of Aqueous cis-Pinonic Acid Photolysis. J. Phys. Chem. A. A 2013, 117, 12930−12945, https://doi.org/10.1021/jp4093018, 2013.

Liu, T., Marlier, M. E., Karambelas, A., Jain, M., Singh, S., Singh, M. K., Gautam, R., and DeFries, R. S.: Missing emissions from post-monsoon agricultural fires in northwestern India: regional limitations of MODIS burned area and active fire products. Environ. Res. Communications 1, 011007, https://doi.org/10.1088/2515-7620/ab056c, 2019.

Liu, Y., Chen, H., Gao, J., Li, Y., Dave, K., Chen, J., Federici, M., and Perricone, G.: Comparative analysis of non-exhaust airborne particles from electric and internal combustion engine vehicles. J. Hazard. Mater. 420, 126626, https://doi.org/10.1016/j.jhazmat.2021.126626, 2021.

Loubet, B., Buysse, P., Gonzaga-Gomez, L., Lafouge, F., Ciuraru, R., Decuq, C., Kammer, J., Bsaibes, S., Boissard, C., Durand, B., Gueudet, J.-C., Fanucci, O., Zurfluh, O., Abis, L., Zannoni, N., Truong, F., Baisnée, D., Sarda-Estève, R., Staudt, M., and Gros, V.: Volatile organic compound fluxes over a winter wheat field by PTR-Qi-TOF-MS and eddy covariance, Atmos. Chem. Phys. 22, 2817–2842, https://doi.org/10.5194/acp-22-2817-2022, 2022.

Lyman WJ.: Estimation of physical properties. In: Neely WB, Blau GE, editors. Environmental Exposure From Chemicals. Boca Raton, FL: CRC Press. p. 13–47, https://doi.org/10.1201/9781351071789, 1985.

Lyman, W. J., Reehl, W. F., and Rosenblatt, D. H.: Handbook of chemical property estimation methods, United States. Available at: https://www.osti.gov/biblio/6942967, 1990.

Mahilang, M., Deb, M. K., Pervez, S., Tiwari, S., and Jain, V. K.: Biogenic secondary organic aerosol formation in an urban area of eastern central India: Seasonal variation, size distribution and source characterization, Environ. Res. 195, 110802, https://doi.org/10.1016/j.envres.2021.110802, 2021.

Mishra, S., Tripathi, S. N., Kanawade, V. P., Haslett, S. L., Dada, L., Ciarelli, G., Kumar, V., Singh, A., Bhattu, D., Rastogi, N., Daellenbach, K. R., Ganguly, D., Gargava, P., Slowik, J. G., Kulmala, M., Mohr, C., El-Haddad, I., and Prevot, A. S. H.: Rapid night-time nanoparticle growth in Delhi driven by biomass-burning emissions. Nat. Geosci. 16(3), 224–230, https://doi.org/10.1038/s41561-023-01138-x, 2023.

Mishra, S., Sinha, V., Hakkim, H., Awasthi, A., Ghude, S. D., Soni, V K.., Nigam, N., Sinha, B., and Rajeevan M.: Biomass burning sources control ambient particulate matter but traffic and industrial sources control VOCs and secondary pollutant formation during extreme pollution events in Delhi, Atmos. Chem. Phys. Discuss., (submitted), 2024.

Mochizuki, T., Kawamura, K., Miyazaki, Y., Kunwar, B., and Boreddy, S. K. R.: Distributions and sources of low-molecular-weight monocarboxylic acids in gas and particles from a deciduous broadleaf forest in northern Japan. Atmos. Chem. Phys., 19(4), 2421-2432, https://doi.org/10.5194/acp-19-2421-2019, 2019.

Nagar, P.K., Singh, D., Sharma, M., Kumar, A., Aneja, V. P., George, M. P., Agarwal, N., Shukla, S. P.: Characterization of PM2.5 in Delhi: role and impact of secondary aerosol, burning of biomass, and municipal solid waste and crustal matter. Environ. Sci. Pollut. Res. 24:25179–25189, https://doi.org/10.1007/s11356-017-0171-3, 2017.

Nagpure, A. S., Ramaswami, A., and Russell, A.: Characterizing the spatial and temporal patterns of open burning of municipal solid waste (MSW) in Indian cities. Environ. Sci. Technol. 49, 12904–12912, https://doi.org/10.1021/acs.est.5b03243, 2015.

Nagpure, A. S., Gurjar, B. R., Kumar, V., Kumar, P.: Estimation of exhaust and non-exhaust gaseous, particulate matter and air toxics emissions from on-road vehicles in Delhi. Atmos. Environ. 127, 118–124, https://doi.org/10.1016/j.atmosenv.2015.12.026, 2016.

Norris, G., Duvall, R., Brown, S., and Bai, S.: EPA Positive Matrix Factorization (PMF) 5.0 Fundamentals and User Guide, available at: https://www.epa.gov/sites/production/files/2015-02/documents/pmf_5.0_user_guide.pdf (last access: 31 October 2019), 2014.

Nowakowska, M., Herbinet, O., Dufour, A., and Glaude, P. A.: Kinetic Study of the Pyrolysis and Oxidation of Guaiacol. J. Phys. Chem. A, 122(39), 7894–7909, https://doi.org/10.1021/acs.jpca.8b06301, 2018.

Paatero, P., Eberly, S., Brown, S. G., and Norris, G. A.: Methods for estimating uncertainty in factor analytic solutions. Atmos. Meas. Tech. 7(3), 781–797, https://doi.org/10.5194/AMT-7-781-2014, 2014.

Paatero, P., Hopke, P. K., Song, X. H., and Ramadan, Z.: Understanding and controlling rotations in factor analytic models. Chemometr. Intell. Lab.60(1–2), 253–264, https://doi.org/10.1016/S0169-7439(01)00200-3, 2002.

Paatero, P., and Hopke, P. K.: Rotational tools for factor analytic models. J. Chemometrics, 23(2), 91–100, https://doi.org/10.1002/CEM.1197, 2009.

Pagonis, D., Sekimoto, K., and de Gouw, J.: A Library of Proton-Transfer Reactions of H3O+ Ions Used for Trace Gas Detection. J. Am. Soc. Mass Spectrom. 30(7), 1330–1335, https://doi.org/10.1007/S13361-019-02209-3/SUPPL_FILE/JS8B06050_SI_001.XLSX.

Pallavi, Sinha, B., and Sinha, V.: Source apportionment of volatile organic compounds in the northwest Indo-Gangetic Plain using a positive matrix factorization model. Atmos. Chem. Phys., 19(24), 15467–15482, https://doi.org/10.5194/ACP-19-15467-2019, 2019.

Palm, B. B., Peng, Q. Y., Fredrickson, C. D., Lee, B., Garofalo, L. A., Pothier, M. A., Kreidenweis, S. M., Farmer, D. K., Pokhrel, R. P., Shen, Y. J., Murphy, S. M., Permar, W., Hu, L., Campos, T. L., Hall, S. R., Ullmann, K., Zhang, X., Flocke, F., Fischer, E. V., and Thornton, J. A.: Quantification of organic aerosol and brown carbon evolution in fresh wildfire plumes, P. Natl. Acad. Sci. USA, 117, 29469–29477, https://doi.org/10.1073/pnas.2012218117, 2020.

Pandey, A., Brauer, M., Cropper, M. L., Balakrishnan, K., Mathur, P., Dey, S., Turkgulu, B., Kumar, G. A., Khare, M., Beig, G., Gupta, T., Krishnankutty, R. P., Causey, K., Cohen, A. J., Bhargava, S., Aggarwal, A. N., Agrawal, A., Awasthi, S., Bennitt, F., … Dandona, L.: Health and economic impact of air pollution in the states of India: the Global Burden of Disease Study 2019. The Lancet Planetary Health, 5(1), e25–e38, https://doi.org/10.1016/S2542-5196(20)30298-9, 2021.

Park, J.-H., Goldstein, A. H., Timkovsky, J., Fares, S., Weber, R., Karlik, J., and Holzinger, R.: Eddy covariance emission and deposition flux measurements using proton transfer reaction – time of flight – mass spectrometry (PTR-TOF-MS): comparison with PTR-MS measured vertical gradients and fluxes. Atmos. Chem. Phys. 13, 1439–1456, https://doi.org/10.5194/acp-13-1439-2013, 2013.

Pawar, H., Garg, S., Kumar, V., Sachan, H., Arya, R., Sarkar, C., Chandra,B. P. and Sinha, B.: Quantifying the contribution of long-range transport to Particulate Matter (PM) mass loadings at a suburban site in the North-Western Indo Gangetic Plain (IGP). Atmos. Chem. Phys. 15, 9501–9520, 2015, https://doi.org/10.5194/ACP-15-9501-2015, 2015.

Pawar, H., and Sinha, B.: Residential heating emissions (can) exceed paddy-residue burning emissions in rural northwest India. Atmos. Environ. 269, 118846, https://doi.org/10.1016/J.ATMOSENV.2021.118846, 2022.

Portillo-Estrada, M., Kazantsev, T., Talts, E., Tosens, T., Niinemets, Ü.: Emission Timetable and Quantitative Patterns of Wound-Induced Volatiles Across Different Leaf Damage Treatments in Aspen (Populus Tremula). J Chem Ecol 41:1105–1117, https://doi.org/10.1007/s10886-015-0646-y, 2015.

Prakash, J., Choudhary, S., Raliya, R., Chadha, T. S., Fang, J., and Biswas, P.: Real-time source apportionment of fine particle inorganic and organic constituents at an urban site in Delhi city: An IoT-based approach. Atmos. Pollut. Res. 12(11), https://doi.org/10.1016/j.apr.2021.101206, 2021.

Ramasamy, S., Nakayama, T., Imamura, T., Morino, Y., Kajii, Y., and Sato, K.: Investigation of dark condition nitrate radical- and ozone-initiated aging of toluene secondary organic aerosol: Importance of nitrate radical reactions with phenolic products. Atmos. Environ. 219, 117049, https://doi.org/10.1016/j.atmosenv.2019.117049, 2019.

Reyes-Villegas, E., Panda, U., Darbyshire, E., Cash, J. M., Joshi, R., Langford, B., Di Marco, C. F., Mullinger, N. J., Alam, M. S., Crilley, L. R., Rooney, D. J., Acton, W. J. F., Drysdale, W., Nemitz, E., Flynn, M., Voliotis, A., McFig.gans, G., Coe, H., Lee, J., Hewitt, C. N., Heal, M. R., Gunthe, S. S., Mandal, T. K., Gurjar, B. R., Shivani, Gadi, R., Singh, S., Soni, V., and Allan, J. D.: PM1 composition and source apportionment at two sites in Delhi, India, across multiple seasons. Atmos. Chem. Phys. 21, 11655–11667, https://doi.org/10.5194/acp-21-11655-2021, 2021.

Rizzo, M. J., and Scheff, P. A.: Utilizing the Chemical Mass Balance and Positive Matrix Factorization models to determine influential species and examine possible rotations in receptor modeling results. Atmos. Environ. 41(33), 6986–6998, https://doi.org/10.1016/J.ATMOSENV.2007.05.008, 2007.

Rolph, G., Stein, A., and Stunder, B.: Real-time Environmental Applications and Display sYstem: READY. Environmental Modelling and Software 95, 210-228, https://doi.org/10.1016/j.envsoft.2017.06.025, 2017.

Roozitalab, B., Carmichael, G.R., and Guttikunda, S.K.: Improving regional air quality predictions in the Indo-Gangetic Plain – case study of an intensive pollution episode in November 2017. Atmos. Chem. Phys. 21, 2837–2860. https://doi.org/10.5194/acp-21-2837-2021, 2021.

Sarkar, C., Sinha, V., Kumar, V., Rupakheti, M., Panday, A., Mahata, K. S., Rupakheti, D., Kathayat, B., and Lawrence, M. G.: Overview of VOC emissions and chemistry from PTR-TOFMS measurements during the SusKat-ABC campaign: high acetaldehyde, isoprene and isocyanic acid in wintertime air of the Kathmandu Valley. Atmos. Chem. Phys. 16, 3979–4003, https://doi.org/10.5194/acp-16-3979-2016, 2016.

Sarkar, C., Sinha, V., Sinha, B., Panday, A. K., Rupakheti, M., and Lawrence, M. G.: Source apportionment of NMVOCs in the Kathmandu Valley during the SusKat-ABC international field campaign using positive matrix factorization. Atmos. Chem. Phys. 17(13), 8129–8156, https://doi.org/10.5194/ACP-17-8129-2017, 2017.

Sharma, S. K., Sharma, A., Saxena, M., Choudhary, N., Masiwal, R., Mandal, T. K., and Sharma, C.: Chemical characterization and source apportionment of aerosol at an urban area of Central Delhi, India. Atmos. Pollut. Res. 7(1), 110–121, https://doi.org/10.1016/j.apr.2015.08.002, 2016.

Sharma, S.K. and Mandal T.K.: Chemical composition of fine mode particulate matter (PM2.5) in an urban area of Delhi, India and its source apportionment. Urban Climate 21, 106–122, https://doi.org/10.1016/j.uclim.2017.05.009, 2017.

Sharma, G., Annadate, S., and Sinha, B.: Will open waste burning become India's largest air pollution source? Environ. Pollut. 292, 118310, https://doi.org/10.1016/j.envpol.2021.118310, 2022.

Shukla, A. K., Tripathi, S. N., Canonaco, F., Lalchandani, V., Sahu, R., Srivastava, D., Dave, J., Thamban, N. M., Gaddamidi, S., Sahu, L., Kumar, M., Singh, V., and Rastogi, N.: Spatio-temporal variation of C-PM2.5 (composition based PM2.5) sources using PMF*PMF (double-PMF) and single-combined PMF technique on real-time non-refractory, BC and elemental measurements during post-monsoon and winter at two sites in Delhi, India. Atmos. Environ. 293, 119456, https://doi.org/10.1016/j.atmosenv.2022.119456, 2023.

Sinha, V., Kumar, V., and Sarkar, C.: Chemical composition of pre-monsoon air in the Indo-Gangetic Plain measured using a new air quality facility and PTR-MS: High surface ozone and strong influence of biomass burning. Atmos. Chem. Phys. 14(12), 5921–5941, https://doi.org/10.5194/ACP-14-5921-2014, 2014.

Singh, R., Sinha, B., Hakkim, H., and Sinha, V.: Source apportionment of volatile organic compounds during paddy-residue burning season in north-west India reveals a large pool of photochemically formed air toxics. Environ. Pollut. 338, 122656, https://doi.org/10.1016/j.envpol.2023.122656, 2023.

Srivastava, A., Gupta, S., and Jain, V. K.: Source Apportionment of Total Suspended Particulate Matter in Coarse and Fine Size Ranges Over Delhi. Aerosol Air Qual. Res. 8, 188-200, https://doi.org/10.4209/aaqr.2007.09.0040, 2008.

Stein, A.F., Draxler, R.R, Rolph, G.D., Stunder, B.J.B., Cohen, M.D., and Ngan, F.: NOAA's HYSPLIT atmospheric transport and dispersion modeling system. Bull. Amer. Meteor. Soc., 96, 2059-2077, https://doi.org/10.1175/BAMS-D-14-00110.1, 2015

Stockwell, C. E., Veres, P.R., Williams, J. and Yokelson, R.J.: Characterization of biomass burning emissions from cooking fires, peat, crop residue, and other fuels with high-resolution proton-transfer-reaction time-of-flight mass spectrometry. Atmos. Chem. Phys. 15, 845–865, https://doi.org/10.5194/acp-15-845-2015, 2015.

https://doi.org/10.5194/egusphere-2024-501
Preprint. Discussion started: 23 February 2024

Thakur, M.: Low-smoke chulha and health consequences in Indian slums. [Doctoral Thesis, Maastricht University]. Maastricht University, https://doi.org/10.26481/dis.20230403mt, 2023.

Wang, M., Wang, Q., Ho, S. S. H., Li, H., Zhang, R., Ran, W., Que, L.: Chemical characteristics and sources of nitrogen-containing organic compounds at a regional site in the North China Plain during the transition period of autumn and winter. Sci. Total. Environ. 812, 151451, https://doi.org/10.1016/j.scitotenv.2021.151451, 2022.

Wiedinmyer, C., Kimura, Y., McDonald-Buller, E. C., Emmons, L. K., Buchholz, R. R., Tang, W., Seto, K., Joseph, M. B., Barsanti, K. C., Carlton, A. G., and Yokelson, R.: The Fire Inventory from NCAR version 2.5: an updated global fire emissions model for climate and chemistry applications, Geosci. Model Dev., 16, 3873–3891, https://doi.org/10.5194/gmd-16-3873-2023, 2023.

Xu, C., GaoL., Lyu, C., Qiao, L. Huang, D., Liu, Y., Li, D. and Zheng, M.: Molecular characteristics, sources and environmental risk of aromatic compounds in particulate matter during COVID-2019: Nontarget screening by ultra-high resolution mass spectrometry and comprehensive two-dimensional gas chromatography. Environ. Int. 167 107421, https://doi.org/10.1016/j.envint.2022.107421, 2022.

Yáñez-Serrano, A. M., Filella, I., LLusià, J., Gargallo-Garriga, A., Granda, V., Bourtsoukidis, E., Williams, J., Seco, R., Cappellin, L., Werner, C., de Gouw, J., and Peñuelas, J.: GLOVOCS - Master compound assignment guide for proton transfer reaction mass spectrometry users. Atmos. Environ. 244, 117929, https://doi.org/10.1016/J.ATMOSENV.2020.117929, 2021.

Yao, L., Wang, M.-Y., Wang, X. -K. Liu, Y.-J., Chen, H.-F., Zheng, J., Nie, W., Ding, A.-J., Geng, F.-H., Wang, D.-F., Chen, J.-M., Worsnop, D. R. and Wang, L.: Detection of atmospheric gaseous amines and amides by a high-resolution time-of-flight chemical ionization mass spectrometer with protonated ethanol reagent ions. Atmos. Chem. Phys., 16, 14527–14543. https://doi.org/10.5194/acp-16-14527-2016, 2016.

You, Y., Kanawade, V. P., de Gouw, J. A., Guenther, A. B., Madronich, S., Sierra-Hernández, M. R., Lawler, M., Smith, J. N., Takahama, S., Ruggeri, G., Koss, A., Olson, K., Baumann, K., Weber, R. J., Nenes, A., Guo, H., Edgerton, E. S., Porcelli, L., Brune, W. H., Goldstein, A. H., and Lee, S.-H.: Atmospheric amines and ammonia measured with a chemical ionization mass spectrometer (CIMS). Atmos. Chem. Phys. 14, 12181–12194, https://doi.org/10.5194/acp-14-12181-2014, 2014.

Yuan, B., Shao, M., De Gouw, J., Parrish, D. D., Lu, S., Wang, M., Zeng, L., Zhang, Q., Song, Y., Zhang, J., and Hu, M.: Volatile organic compounds (VOCs) in urban air: How chemistry affects the interpretation of positive matrix factorization (PMF) analysis. J. Geophys. Res-Atmos.117(D24), 24302, https://doi.org/10.1029/2012JD018236, 2012.

Yuan, B., Koss, A.R., Warneke, C., Coggon, M., Sekimoto, K., and de Gouw, J.: Proton-Transfer-Reaction Mass Spectrometry: Applications in Atmospheric Sciences. Chem. Rev. 117 (21), 13187-13229, https://doi.org/10.1021/acs.chemrev.7b00325, 2017.

Zaytsev, A., Koss, A. R., Breitenlechner, M., Krechmer, J. M., Nihill, K. j. Lim, C. Y., Rowe, J. C., Cox, J. L., Moss, J., Roscioli, J. R., Canagaratna, M. R., Worsnop, D. R., Kroll, J. H., and Keutsch1, F. N.: Mechanistic Study of Formation of Ring-retaining and Ring-opening Products from Oxidation of Aromatic Compounds under Urban Atmospheric Conditions. Atmos. Chem. Phys. 19, 15117–15129, https://doi.org/10.5194/acp-19-15117-2019, 2019.